Agricultural Water Management 333 (2026) 110634

Contents lists available at ScienceDirect

Agricultural Water Management

journal homepage: www.elsevier.com/locate/agwat

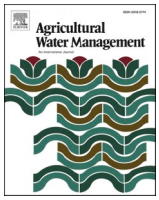

Linking plant water status dynamics to yield and fruit cracking in citrus orchards using UAV multi-sensor data and machine learning

Moshe (Vladislav) Dubinin [a], Michael Morozov [b], Ohaliav Keisar [c], Guy Lidor [c], Victor Alchanatis [c], Avi Sadka [b], Tarin Paz-Kagan [a,*]

[a] French Associates Institute for Agriculture and Biotechnology of Dryland, The Jacob Blaustein Institutes for Desert Research, Ben-Gurion University of the Negev, Sede Boqer Campus, 8499000, Israel
[b] Institute of Plant Sciences, Volcani Agricultural Research Institute, HaMakabim st. 68, Rishon LeZion, 7505101, Israel
[c] Institute of Agricultural and Biosystems Engineering, Volcani Agricultural Research Institute, HaMakabim St. 68, Rishon LeZion, 7505101, Israel

ARTICLE INFO

Keywords:
UAV
LiDAR
thermal
multispectral
plant water status
citrus cracking

ABSTRACT

Citrus fruit cracking causes substantial yield and economic losses, yet its relationship with plant water status (PWS) and irrigation management remains insufficiently characterized. Unlike previous UAV-based irrigation studies that focused on water-stress detection or yield estimation, this study introduces a dynamic, physiology-based framework that links temporal PWS trajectories during key phenological stages to fruit-cracking risk at the individual-tree scale. UAV-based multispectral, thermal, and LiDAR data, combined with field physiological measurements and machine-learning models, were evaluated in an irrigation management experiment in an 'Ori' mandarin orchard (Israel) across three contrasting growing seasons (2023–2025). Several irrigation treatments with different irrigation timings and water inputs were applied during the growing season to evaluate their effects on temporal PWS dynamics and fruit cracking. Trunk growth (TG), stem water potential (SWP), stomatal conductance (SC), and plant area index (PAI) were measured throughout the two seasons and estimated using Random Forest models ($R^2 > 0.783$). These indicators were subsequently used to predict yield and fruit cracking with high accuracy (yield: $R^2 = 0.896$; cracking: $R^2 = 0.845$). Cracking was lowest in 2023 (~3%), with ~25% lower irrigation, suggesting reduced irrigation may reduce cracking risk. Higher cracking in 2024 (~14%, vs ~8% in 2025) coincided with intense heat events. Mid-season SWP and SC were strongly associated with yield formation and cracking patterns. These findings demonstrate that monitoring temporal PWS dynamics can support precision irrigation management by identifying high-risk zones and enabling irrigation strategies that stabilize PWS, reduce the incidence of cracking, and improve yield under variable climatic conditions.

1. Introduction

Cracking is a major agricultural problem affecting many fruit crops, including pomegranate, citrus, grape, cherry, tomato, pear, and litchi (Santos et al., 2023). It is a physiological disorder caused by an imbalance in growth between the pulp and peel. When pulp expansion exceeds the mechanical capacity of the peel, radial or longitudinal cracks develop ((Seo et al., 2022; Santos et al., 2023). Cracking severity is strongly associated with high water availability, which increases pulp turgor pressure relative to peel strength (Fischer, Balaguera-López, and Álvarez-Herrera, 2021; Galindo et al., 2014; Spada et al., 2024). Rapid fluctuations in water availability, high humidity, and elevated air temperature can further intensify cracking. The disorder causes major economic losses by reducing marketable yield and increasing susceptibility to postharvest decay (Seo et al., 2022; Santos et al., 2023; Li and Chen, 2017).

Abbreviation: PWS, Plant Water Status; TG, Trunk Growth; MDS, Maximum Daily Shrinkage; SWP, Stem Water Potential; SC, Stomatal Conductance; PAI, Plant Area Index; PA, Plant Area; UAV, Unmanned Aerial Vehicle; ML, Machine Learning; RF, Random Forest; XGBoost, Extreme Gradient Boosting; ANN, Artificial Neural Network; SVR, Support Vector Regression; Tc, Canopy Temperature; CWSI, Crop Water Stress Index; VPD, Vapor Pressure Deficit; GDD, Growing Degree Days; VI, Vegetation Index; VIP, Variable Importance In Projection; RMSE, Root Mean Square Error; LAD, Leaf Area Density; LiDAR, Light Detection and Ranging; VIF, Variance Inflation Factor; IQR, Interquartile Range.

* Corresponding author.
E-mail address: tarin@bgu.ac.il (T. Paz-Kagan).

https://doi.org/10.1016/j.agwat.2026.110634
Received 15 April 2026; Received in revised form 5 July 2026; Accepted 8 July 2026
Available online 17 July 2026
0378-3774/© 2026 The Authors. Published by Elsevier B.V. This is an open access article under the CC BY-NC-ND license (http://creativecommons.org/licenses/by-nc-nd/4.0/).

In citrus, fruit cracking typically begins about four months after fruit set and peaks between September and November during the cell enlargement stage, when rapid pulp expansion exerts mechanical pressure on the rind (Abekasis et al., 2024; Zur et al., 2017). Cracks usually initiate at the stylar end and extend through the albedo, damaging vascular tissues and often leading to fruit splitting and drop (García-Luis et al., 1994; Abekasis et al., 2024). These cracking processes are closely linked to plant water status (PWS), fruit turgor dynamics, and environmental variability (García-Luis et al., 1994; Abekasis et al., 2024; Mesejo et al., 2016). Cracking severity is influenced by cultivar traits, irrigation management, and environmental stresses such as heatwaves, drought, and heavy rainfall (Galindo et al., 2014; Singh, Shukla, and Meghwal, 2020; Choi et al., 2020; Spada et al., 2024). When the vapor pressure deficit (VPD) falls sharply, cracking intensity is induced in association with inhibited transpiration and induced water flow into the fruit (Li and Chen, 2017). Moderate irrigation deficits may reduce cracking by stabilizing PWS and limiting abrupt fluctuations in fruit turgor (Cronjé, Stander, and Theron, 2013; Krajewski et al., 2022). Irrigation frequency also affects cracking intensity, with lower frequency inducing it (Mesejo et al., 2016). Despite extensive research, the temporal relationships among PWS dynamics, environmental forcing, irrigation application, and cracking development remain insufficiently quantified at the orchard scale (Blanco et al., 2022; Singh el al., 2020; Fischer et al., 2021; Shi et al., 2025).

These contrasting effects of water availability on cracking highlight the importance of PWS dynamics throughout the stages of fruit development. PWS reflects the balance between water availability and atmospheric demand and is governed by water-potential gradients, hydraulic functioning, and plant traits (Morris et al., 1998; Nehemy et al., 2019). Common physiological indicators of PWS include trunk maximal daily shrinkage (MDS), trunk growth (TG), stem water potential (SWP), stomatal conductance (SC), and plant area index (PAI). MDS and TG reflect short-term hydraulic responses and changes in living tissues within the phloem and xylem (Dietrich et al., 2018; Steppe et al., 2006; Sevanto, 2017). SWP integrates the soil–plant–atmosphere continuum by reflecting soil water availability, root uptake, xylem transport, and atmospheric demand (Larcher, 2003; Nehemy et al., 2019). SC captures gas exchange and transpiration dynamics, while PAI represents the transpiring canopy surface area (Kozlowski and Pallardy, 1997). These indicators are widely used in precision irrigation and are strongly associated with plant productivity and yield (Nehemy et al., 2019; Puig-Sirera et al., 2021). Dendrometers for TG and MDS, pressure chambers for SWP, porometers for SC, and optical methods for PAI are labor-intensive, time-sensitive, and typically limited to individual trees (Ziegler et al., 2024; Chatterjee et al., 2025).

These limitations have increased interest in UAV-based multi-sensor remote sensing as a non-destructive and spatially comprehensive approach for monitoring canopy-scale (Wang et al., 2018; Gupta et al., 2024; Dahro, Li, and Liu, 2023; Sharma et al., 2022). Thermal remote sensing is widely used to derive canopy temperature (Tc) and calculate indices such as the Crop Water Stress Index (CWSI) (Idso et al., 1981), which is strongly associated with SWP (Boyaci et al., 2024; Katz et al., 2023). Thermal indicators are highly influenced by atmospheric conditions, particularly air temperature and vapor pressure deficit (VPD), which strongly regulate transpiration and plant water stress (Bo et al., 2023; Boyaci et al., 2024; Hassanpour et al., 2024). Multispectral imagery complements thermal observations by capturing reflectance in the visible, red-edge, and near-infrared regions sensitive to canopy water content, chlorophyll concentration, and stress-related physiological responses (Efrat et al., 2025; Avioz et al., 2025). Thermal and multispectral observations mainly capture canopy surface responses and provide limited information on internal structural and hydraulic dynamics. LiDAR complements these approaches by providing high-resolution information on canopy architecture, including canopy height, density, and plant area index (PAI) (Ahmad et al., 2021; Fang et al., 2019; Ustin and Middleton, 2021). Integrating thermal, multispectral, and LiDAR observations enables a more comprehensive characterization of PWS by jointly capturing canopy physiology and structure (Dorigo et al., 2007; Haboudane et al., 2004).

Advances in machine learning (ML) and UAV remote sensing have improved the ability to monitor PWS, physiological responses, and yield variability at high spatial and temporal resolutions. ML approaches such as Random Forest (RF), XGBoost, artificial neural networks (ANN), and support vector regression (SVR) are increasingly used to integrate multispectral, thermal, LiDAR, meteorological, and physiological data for estimating PWS, irrigation demand, and crop productivity (Romero et al., 2018; Velazquez-Chavez et al., 2024; Cho et al., 2024). UAV-derived multi-sensor observations have been shown to reliably predict seasonal PWS and yield under contrasting irrigation regimes (Sánchez-Virosta et al., 2025; Efrat et al., 2025). Additional studies highlighted the potential of ML approaches for estimating plant stress, soil moisture, and irrigation-related variability in citrus orchards (Liu et al., 2024). Because orchard-scale physiological datasets are often relatively small and contain highly correlated environmental and sensor-derived variables, this study focused on ML models that are robust to moderate sample sizes and nonlinear relationships. RF, XGBoost, SVR, and relatively shallow ANN architectures were selected because they demonstrated strong performance and stability in agricultural remote sensing applications while reducing the risk of overfitting and maintaining model interpretability.

Most previous UAV-based orchard studies focused on (i) water-stress detection and irrigation management using thermal and spectral indicators (Gonzalez-Dugo et al., 2013; Romero et al., 2018; Velazquez-Chavez et al., 2024), (ii) canopy condition and plant water status assessment (Park et al., 2017; Sánchez-Virosta et al., 2025), or (iii) yield prediction using multisensory and machine-learning approaches (Efrat et al., 2025). However, these approaches generally rely on static or single-date measurements and often treat fruit cracking as a secondary end-of-season outcome rather than as a dynamic physiological process. In Citrus, ML approaches have only recently been applied to identify environmental drivers associated with fruit cracking at regional scales (Abekasis et al., 2024), while the relationship between temporally dynamic PWS trajectories and fruit-cracking risk at the individual-tree scale remains poorly quantified. As a result, the relationships among temporal fluctuations in PWS, irrigation timing, atmospheric demand, and cracking-associated yield loss remain insufficiently quantified at the tree and orchard scale. Limited attention has been given to how temporally resolved PWS trajectories during sensitive phenological stages contribute to spatial and interannual variability in fruit-cracking risk under contrasting irrigation and climatic conditions. The novelty of the present study lies in the development of a tree-scale, physiology-based framework that integrates UAV-derived multispectral, thermal, and LiDAR observations with field physiological measurements and ML models to characterize temporal PWS dynamics and relate them to both yield formation and fruit-cracking risk. Rather than using remote sensing only for stress detection or yield prediction, this study evaluates whether temporally resolved PWS indicators can explain spatial and interannual variability in cracking under varied irrigation and climatic conditions.

This study aims to quantify and model the relationships among PWS dynamics, yield formation, and fruit cracking in citrus orchards under varying irrigation and climatic conditions. To achieve this, UAV-based multispectral, thermal, and LiDAR observations were integrated with field physiological measurements and ML approaches within irrigation experiments. The specific objectives were to: (1) estimate key canopy-scale PWS indicators (TG, SWP, SC, and PAI) using UAV-derived multispectral, thermal, LiDAR, and environmental variables under different irrigation applications; (2) predict yield and fruit-cracking incidence using temporally resolved PWS indicators and identify the dominant predictors and their timing during the growing season; (3) quantify the effects of irrigation application and climatic variability, including heatwaves and atmospheric demand, on the temporal evolution of PWS

and associated yield and cracking responses across seasons; and (4) characterize the spatial and temporal heterogeneity of PWS at the tree level and evaluate its relationship with orchard-scale variability in yield and fruit cracking. This framework enables evaluation of fruit cracking as a temporally dynamic physiological response rather than solely as an end-of-season damage outcome.

We hypothesize that fruit cracking is strongly associated with temporal fluctuations and instability in PWS during critical phenological stages rather than with irrigation amount alone. We further hypothesize that the temporal stability of PWS is a primary determinant of fruit-cracking risk and that deficit irrigation, when properly timed, may help maintain this stability without substantially reducing yield. Finally, we hypothesize that spatial and temporal heterogeneity in PWS is a major driver of orchard-scale variability in both yield and fruit cracking, and that these dynamics can be captured by integrating UAV-based multi-sensor observations with environmental drivers.

2. Methods and materials

The methods were organized as a two-stage workflow to separate physiological understanding from spatial upscaling. In the first stage, direct physiological measurements (TG, SWP, SC, and PAI) collected from 24 reference trees were used to quantify the relationships between temporal PWS dynamics, yield, and fruit cracking during key phenological stages. In the second stage, UAV-derived multispectral, thermal, and LiDAR observations were used to estimate these PWS indicators and extend them from a limited number of sampled trees to the entire orchard. The estimated PWS indicators were then used to predict yield and fruit-cracking responses for 72 trees enable orchard-scale spatial analyses, including identifying high-risk zones and clustering tree responses. This hierarchical workflow was designed to demonstrate that UAV-derived PWS indicators can reproduce the physiological relationships observed from field measurements while providing spatially explicit information to support precision irrigation management.

2.1. Plant material and study area

The irrigation experiment was conducted in the central coastal region of Israel, an area known for its Mediterranean climate and citrus cultivation. The study site is a commercial orchard of 19-years old 'Ori' mandarin (*Temple mandarin (Citrus reticulata X C. Sinensis) X Kinnow mandarin (C. nobilis × C. deliciosa)* trees grafted on Sour Orange (*Citrus × aurantium*) rootstock, located near Kfar Chabad in the Lod Valley (31°59'00.4"N, 34°51'38.6"E; Fig. 1). The orchard, containing about 1300 trees covers 1.56 ha, and is planted at a spacing of 6 m between rows and 3.5 m within rows. The region has a typical Mediterranean climate, with a long, dry summer and an average annual rainfall of 550 mm. Irrigation is usually applied between April and November. The experimental plot consisted of 36 orchard rows arranged into four irrigation treatments, each replicated across three randomized blocks (Fig. 2a–b). Treatments included: (1) Control (100%) - irrigation at the recommended level for the area and soil type. (2) Over-irrigation (150%) - continuous application of 150% of the recommended level. (3) Early reduced irrigation (50% early) - Irrigation was reduced to 50% of the control level during the early season (21 May−30 June 2023 and 5 May−26 June 2024). (4) Late reduced irrigation (50% late) - Irrigation was reduced to 50% of the control level during the late season (17 August−14 October 2023 and 29 August−27 October 2024). Irrigation amounts in the control treatment were determined using the Penman-Monteith reference evapotranspiration, following guidelines from Israel's Extension Service, Ministry of Agriculture and Food Security. Locations of sampled trees were precisely mapped using Real-Time Kinematic (RTK) GPS. Monthly UAV flights were conducted throughout

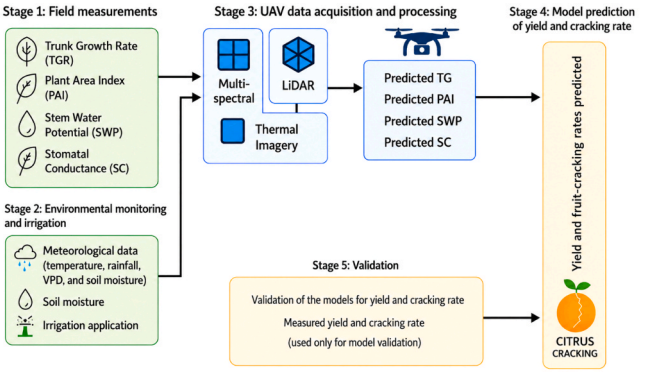

Fig. 2. Conceptual workflow of the multi-stage modeling framework. UAV-derived spectral (multispectral) and thermal features, LiDAR-based structural features, and meteorological and irrigation data were integrated at the individual-tree level across multiple acquisition dates. In the first modeling step, these temporally resolved variables were used to estimate plant water status (PWS) indicators, including trunk growth (TG), stomatal conductance (SC), stem water potential (SWP), and plant area index (PAI), using machine-learning (ML) models (Stage 1-3). In the second step, the derived PWS indicators were used as physiologically meaningful predictors to model total yield and fruit-cracking-related yield loss at tree and plot scales (Stage 4-5).

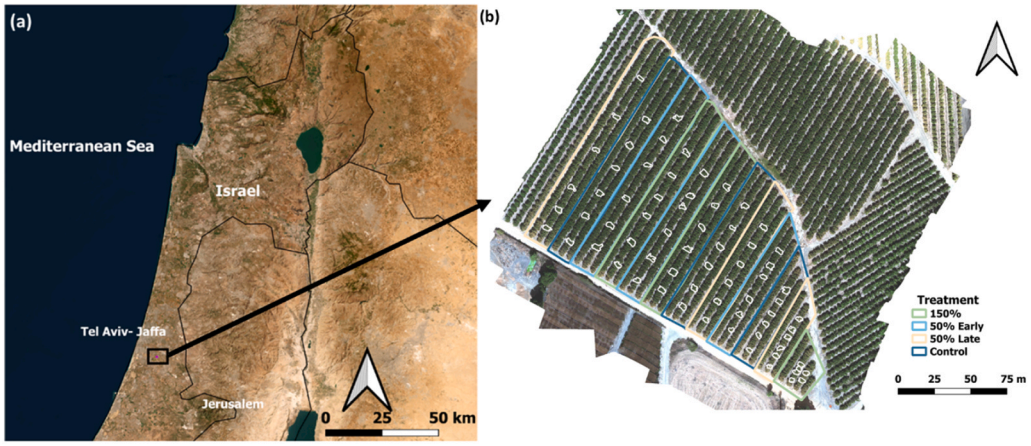

Fig. 1. (a) Location of the study area in Israel; (b) experimental layout of the irrigation treatments within the orchard. The 36 orchard rows were divided into four irrigation treatments, each replicated across three randomized blocks. Colored frames represent the irrigation treatments: green – over-irrigation (150%); light blue – early deficit irrigation (50% early); yellow – late deficit irrigation (50% late); and dark blue – control (100%). White frames indicate sampled trees used for physiological measurements and model calibration.

the 2023–2025 growing seasons using an integrated multi-sensor system that combined LiDAR, thermal, and multispectral sensors.

2.2. Research approach

This study developed ML models to predict fruit cracking and yield based on seasonal tree physiology, specifically PWS. PWS was quantified using four key indicators: TG, SWP, SC, and PAI. Because direct physiological measurements were limited to 24 reference trees, an insufficient sample size for training robust ML models, a hierarchical, two-stage framework to expand the dataset was implemented: (i) Step 1 (PWS Estimation): Field measurements from the 24 reference trees were integrated with UAV observations (multispectral, thermal, and LiDAR), meteorological data, and irrigation records from the 2023–2025 growing seasons. ML models were trained on these inputs to reconstruct and estimate PWS indicators, effectively extrapolating tree physiology across the entire orchard without requiring further direct measurements. (ii) Step 2 (Yield and Cracking Prediction): The continuous PWS estimates were subsequently used to model and predict yield and fruit-cracking outcomes for an expanded dataset of 72 trees, which were monitored under contrasting climatic and irrigation conditions. To execute this framework, the workflow was divided into five sequential stages: (1) Field physiological measurements (24 reference trees). (2) Environmental monitoring (meteorological, irrigation, and soil moisture data). (3) UAV data acquisition and processing. (4) ML-based estimation of PWS indicators. (5) Tree- and orchard-scale modeling of yield and cracking responses (72 trees). All diverse data streams were spatially integrated using LiDAR-derived individual-tree segmentation. This unified tree-level dataset enabled the characterization of seasonal PWS trajectories across key phenological stages, translating remote UAV observations into physiologically meaningful indicators to explain spatial and interannual variability in orchard production outcomes.

Stage 1: Field measurements - Continuous monitoring of TG and MDS was conducted on 24 reference trees to provide ground-truth data for model calibration and validation. In parallel, SWP, SC, and LAI were measured monthly on the same trees for two sessions. Stage 2: Environmental monitoring - Meteorological variables, including air temperature, rainfall, and vapor pressure deficit (VPD), were recorded using an on-site weather station. Irrigation inputs were documented for each treatment, and soil moisture was continuously monitored using in situ sensors. Stage 3: UAV data acquisition and processing - UAV campaigns equipped with multispectral, thermal, and LiDAR sensors were conducted over the orchard. LiDAR point clouds were processed to classify ground returns, normalize canopy height, and segment individual trees. LiDAR-derived individual-tree segmentation polygons were used as the common spatial framework for integrating multispectral, thermal, structural, meteorological, irrigation, and field physiological data into a unified tree-level dataset linked by tree ID and acquisition date. For each tree polygon, spectral reflectance and vegetation indices were derived from multispectral imagery, while canopy temperature (Tc) and the CWSI were extracted from thermal data. Stage 4: ML modeling- ML models were trained using UAV-derived spectral, thermal, and structural variables, along with meteorological and irrigation data, to estimate TG, SWP, and SC across the orchard. PAI was derived directly from LiDAR data using leaf area density profiles and projected canopy area and validated against field measurements. Stage 5: Yield and fruit-cracking analysis - PWS indicators from key phenological periods were related to yield and fruit-cracking rates using ML models.

This hierarchical approach reduces dimensionality and links model outputs more directly to plant-level physiological processes rather than raw sensor inputs. In addition, unsupervised clustering based on observed yield and fruit-cracking metrics was used to identify distinct spatial and temporal response patterns within the orchard. These clusters were subsequently related to PWS dynamics to support the interpretation of management- and environment-driven stress patterns. A summary of variables, data sources, and calculation methods is provided in Table S1.

2.3. Meteorological and soil moisture data

Meteorological data for the study area were obtained from the Kfar Chabad station (34.833199°E, 31.980801°N; elevation 59 m), one of the stations operated by the Ministry of Agriculture and Food Security of Israel, with data available at https://www.agrometeorology.co.il/. The dataset included air temperature (°C), relative humidity (RH, %), precipitation (mm day^{-1}), and growing degree days (GDD). Heatwave periods were identified according to the Israeli Meteorological Service (IMS) definition of the Eastern Mediterranean climate. According to this definition, a heatwave consists of at least three consecutive days with midday maximum temperatures of 32–35 °C, nighttime maximum temperatures of 28–29 °C, relative humidity above 50% at noon, and 80–90% at midnight (Robinson, 2001). In addition to meteorological records, soil volumetric water content was continuously monitored using 12 sensors installed at depths of 15, 30, 45, and 60 cm across the study plots, distributed among the different irrigation treatments (Phytech, LTD, Kfar Saba, Israel).

2.4. PWS field measurements

Trunk diameter was continuously monitored using dendrometers (Phytech© Ltd., Kfar Saba, Israel; https://www.phytech.com) installed on 24 trees representing the four irrigation treatments (Fig. 1). These measurements were used to derive TG and MDS. Midday SWP was measured immediately following each UAV data acquisition using a pressure chamber. Midday SWP was measured immediately after each UAV data acquisition session using a pressure chamber (Arimad 3000, MRC, Holon, Israel) on 24 sampled trees, following established protocols (Nemera et al., 2023). SC on 24 sampled trees was measured between 09:00 and 11:00 h using a portable photosynthesis system (LI−6400XT; LI-COR Inc., Lincoln, NE, USA). Measurements were conducted on fully expanded leaves under standardized conditions: photosynthetic photon flux density of 1000 μmol m^{-2} s^{-1} , flow rate of 500 μmol s^{-1} , and leaf chamber temperature of 25 °C. PAI was measured around midday (12:00) using the SS1 SunScan Canopy Analysis System (Delta-T Devices, UK). Measurements were taken under clear-sky conditions to minimize the effects of clouds (Ogunbadewa, 2012). For each tree, four readings were collected from the south, west, north, and east sides and averaged to obtain a representative PAI value that incorporates both leaf and woody canopy components.

2.5. Yield and fruit cracking

During the fruit-cracking period (September–December), cracked fruits were manually counted on each of the 72 monitored trees, including the 24 intensively sampled trees, at 3–4-week intervals. To prevent double-counting, all recorded cracked fruits were removed from the trees or under them, if dropped. At commercial harvest, the total number of fruits per tree was recorded, and the percentage of fruit cracking was calculated as the ratio of cracked fruits to the total fruit number. In addition, total fruit weight per tree was measured to quantify yield as biomass.

2.6. Remote sensing UAV

Data were collected during 19 UAV flight campaigns conducted over three growing seasons (2022–2023, 2023–2024 and 2024–2025; Table S2), acquiring multispectral, thermal, and LiDAR data. Flights were conducted around midday (≈12:00) at an altitude of 40 m above ground level, yielding a spatial resolution of approximately 2–5 cm. The UAV platform (DJI Matrice 600) was equipped with three sensors. A multispectral camera (RedEdge-M, MicaSense, USA) recorded reflectance in five spectral bands: blue (475 nm, 32 nm bandwidth), green

(560 nm, 27 nm), red (668 nm, 14 nm), red-edge (717 nm, 12 nm), and near-infrared (840 nm, 57 nm). Radiometric calibration was performed using standard MicaSense calibration procedures to convert raw digital numbers to surface reflectance, followed by empirical line normalization across flight campaigns to ensure temporal consistency. A thermal camera (A655sc, FLIR Systems, USA; 7.5–14 μm) provided radiometric measurements of canopy temperature (Tc). Thermal data were processed to retrieve surface temperature using sensor-specific calibration, and canopy temperature metrics were derived from vegetation pixels only to minimize background effects. A LiDAR sensor (DJI Zenmuse H20) acquired high-density 3D point clouds (~1250 points m^{-2}), enabling detailed characterization of canopy structure, including tree height, crown area, and PAI. Point clouds were processed through ground classification, height normalization, and tree segmentation to derive plot- and tree-level structural metrics.

Multispectral image processing began by converting raw digital numbers to surface reflectance using the standard MicaSense radiometric calibration protocol, applied to each flight campaign. To ensure temporal consistency across campaigns, an empirical line normalization was subsequently applied (Kizel et al., 2017). A reference image from June 2023, characterized by high spectral variability across the orchard, was selected as the normalization baseline. For each spectral band, six stable reference targets representing bright, dark, and intermediate reflectance levels were identified within the scene. Linear regression models were then used to adjust the reflectance values of all other images to match the reference image. This two-step calibration approach (sensor-based radiometric calibration followed by empirical normalization) ensured consistency of reflectance values across dates and seasons. Following calibration, 14 vegetation indices (VIs) were computed (Table S1), including indices sensitive to canopy chlorophyll and nitrogen status (e.g., NDVI, NDRE) and water stress (e.g., GNDVI and red-edge-based indices). These spectral features were combined with LiDAR-derived structural metrics to form the multi-sensor dataset used for subsequent ML analyses.

Thermal imagery was processed to retrieve radiometric canopy temperature (Tc) using sensor-specific calibration and thermographic processing tools (Tattersall, 2017). Canopy temperature was derived from vegetation pixels only, following masking of non-vegetated surfaces to minimize background effects. The Crop Water Stress Index (CWSI) was calculated according to Eq. 1:

$$CWSI = \frac{(Tc - Ta) - Twet}{Tdry - Twet} \quad (1)$$

where $T_a$is air temperature, T_{wet}represents the lower baseline corresponding to well-watered, fully transpiring canopy conditions, and T_{dry}represents the upper baseline corresponding to non-transpiring or severely stressed canopy conditions (Gonzalez-Dugo et al. 2014; Efrat et al., 2025). This normalization accounts for atmospheric demand and enables comparison of canopy temperature across varying environmental conditions. The $T_{wet}$and T_{dry}baselines were estimated from the distribution of $T_c - T_a$values within vegetation pixels for each flight, using the 2.5th and 97.5th percentiles, respectively. This approach is consistent with empirical CWSI formulations, where the lower and upper limits represent the extremes of fully transpiring and non-transpiring canopy states (Katimbo et al. 2022). The use of percentile-based thresholds reduces sensitivity to noise and outliers while capturing the effective range of canopy thermal responses under field conditions. CWSI is a dimensionless index that typically ranges from 0 (well-watered) to 1 (severely stressed), although values outside this range may occur due to environmental variability or uncertainties in baseline estimates (Katimbo et al. 2022). Importantly, the accuracy of CWSI strongly depends on the correct determination of the upper and lower baselines, which are known to vary with crop type, phenological stage, and atmospheric conditions (Katimbo et al. 2022).

LiDAR point clouds were processed through three main steps: ground classification, height normalization, and tree segmentation. Ground points were identified using the Progressive Morphological Filter (Zhang et al., 2003) to generate a digital elevation model (DEM). Heights were then normalized relative to ground level using a triangulated irregular network (TIN) approach (Roussel et al., 2020). A canopy height model (CHM) was subsequently derived by subtracting the digital surface model (DSM) from the DEM. Individual trees were segmented from the CHM using a watershed-based algorithm (Arrish and Suliman, 2014). The segmentation was further refined using structural constraints, including canopy area, crown diameter, and tree spacing, with manual corrections applied where necessary to improve delineation accuracy. This workflow enabled robust tree-level extraction of structural metrics, including canopy height, crown area, and PAI.

2.7. Estimation of plant area index (PAI) using leaf area density (LAD)

LiDAR point clouds were masked using tree polygons derived from the segmentation procedure, allowing each point to be associated with a unique tree ID and enabling tree-level analysis of structural attributes. For each tree, the leaf area density (LAD) profile was estimated vertically, with the lower boundary defined at 0.5 m above ground to exclude ground and near-surface noise (Li et al., 2017; Wang and Fang, 2020; Roussel et al., 2020). The LAD profile was derived from the gap-fraction profile, which represents the proportion of open sky visible through the canopy. Gap fraction values were converted to LAD using the Beer-Lambert law with an extinction coefficient (k; Roussel et al. 2020). The extinction coefficient was set to 0.4, based on calibration against ground-based PAI measurements obtained using a SunScan system (Roussel et al. 2020). PAI was calculated by integrating the LAD profile over the vertical. In this study, we focused on estimating PAI rather than LAI, as current LiDAR-based methods do not separate woody components (branches and stems) from leaves in citrus canopies. Consequently, PAI includes both photosynthetic and non-photosynthetic elements. PAI showed a strong correlation with field-based measurements ($R^2 = 0.93$; Fig. S1). PAI therefore provides a robust proxy for canopy structure, light interception, and transpiration potential (Fang et al. 2019), and is suitable for integration with spectral and thermal indicators in subsequent analyses. In addition, we calculated plant area (PA), which represents the absolute canopy area of an individual tree (m^2), whereas PAI is a normalized index (m^2 m^{-2}) describing canopy density per unit ground area.

2.8. ML models for estimating plant water status indicators

A performance comparison was conducted among four ML models, Random Forest (RF), Extreme Gradient Boosting (XGBoost), Artificial Neural Networks (ANN), and Support Vector Regression (SVR), to estimate PWS indicators of SC, SWP, and TG. All models were implemented within a unified framework to ensure consistent data handling, training, and evaluation. These models were selected because they are well-suited to medium-sized agricultural datasets, can capture nonlinear relationships among environmental and sensor-derived variables, and have demonstrated stable performance in remote sensing applications. RF is an ensemble learning method that constructs multiple decision trees and aggregates their predictions, reducing overfitting while capturing nonlinear relationships (Matsuki et al., 2016). XGBoost is a regularized gradient-boosting algorithm that builds trees sequentially to minimize prediction error (Friedman, 2001). ANN models serve as flexible nonlinear function approximators (Hornik et al., 1989), while SVR is a kernel-based regression approach that balances model complexity and generalization (Drucker et al., 2003). All models were trained using the same set of predictors to enable a fair comparison.

Hyperparameters were optimized using a 10-fold cross-validation grid search (k = 10) on the calibration (training) dataset. For RF, ntree (10−100) and mtry (2−4) were tuned. For XGBoost, nrounds (10−100), max_depth (2−4), eta (0.1–0.5), gamma (0−1),

colsample_bytree (0−1), and min_child_weight (1−5) were optimized. For ANN, the number of hidden units (size = 1–5) and weight decay (decay = 0.0001–0.1) were tuned. For SVR, radial kernel parameters sigma (0−100) and cost (C = 0–100) were optimized. To minimize redundancy and improve model parsimony, two complementary feature-selection approaches were applied. First, feature selection was performed using the Boruta algorithm (Kursa and Rudnicki, 2010), to identify the most informative predictors, improve model interpretability, reduce redundancy among correlated variables, and minimize the risk of overfitting in the ML models. Boruta algorithm, which is an RF-based wrapper method, was used to identify all relevant predictors by comparing original features with permuted "shadow" features. Boruta focuses on variable relevance and retains predictors that significantly contribute to model performance (Kursa et al., 2010). Second, the variance inflation factor (VIF) analysis (Groß 2003) was applied with a VIF threshold of$>$ 10 to detect and remove multicollinearity among spectral, thermal, structural, and climatic variables. Unlike Boruta, which evaluates predictor importance, VIF evaluates statistical redundancy among predictors. Thus, the two methods were used sequentially to retain informative variables while reducing collinearity and redundancy within the predictor set. The final predictors selected for TG, SWP, SC, yield, and fruit cracking after Boruta feature selection and VIF-based collinearity filtering are summarized in Table S3.

Model performance was evaluated using the coefficient of determination (R^2) and root mean square error (RMSE) for calibration, validation, and test subsets, as well as cross-validation. All field-based PWS indicator measurements and UAV-derived features were integrated into a single dataset and randomly divided into training (70%) and validation (30%) subsets (Table S3). Data from the control irrigation plots, which were excluded from model training, were used as an independent test dataset to assess model robustness and generalization under operational field conditions (Table S4). For each final model, variable importance in projection (VIP) scores were calculated to quantify the relative contribution of spectral, thermal, LiDAR-derived, and meteorological predictors. All ML models were developed in R (R Core, 2026) using the caret package (Kuhn, 2015). Prior to modeling, the dataset underwent quality-control screening to remove observations affected by sensor errors, missing values, or biologically implausible measurements. Valid extreme values were retained because they may represent meaningful physiological stress responses. Potential outliers were identified using the interquartile range (IQR) method, flagging observations below Q1 − 1.5 × IQR or above Q3 + 1.5 × IQR for inspection. Values were removed only when they reflected measurement error or sensor malfunction; biologically plausible extreme values were retained (Tukey, 1977; Hoaglin and Iglewicz, 1987).

2.9. ML models for estimating yield and cracking-associated yield loss

Yield measurements, fruit-cracking observations, and predicted PWS indicators (TG, SC, SWP, and PAI) were integrated into a unified tree-level dataset. To avoid redundancy, the same training and evaluation framework described above (Section 2.7) was applied here. Briefly, the dataset was randomly divided into calibration (70%) and validation (30%) subsets, and model hyperparameters were optimized using 10-fold cross-validation (k = 10). An independent test (prediction) dataset, consisting of control irrigation plots excluded from model calibration, was used to assess model generalization under operational field conditions (Table S4). To further evaluate model robustness and temporal generalization, an additional independent dataset collected during the 2025 growing season was incorporated as an external test set for yield and fruit-cracking prediction. Fruit cracking was modeled as a continuous response variable; therefore, the interannual differences in cracking intensity between 2023 and 2025 were treated as biologically meaningful seasonal variability rather than as a class-imbalance problem. All four models (RF, XGBoost, ANN, and SVR) were implemented consistently using the same framework (*caret* package in R; Kuhn, 2015), and their performance is reported in Table S4. ML models were developed to predict total yield and cracking-associated yield loss at both tree and plot scales.

In contrast to the PWS models, which used spectral, thermal, structural, and climatic variables as predictors, the yield and cracking models were based on derived PWS indicators (TG, SC, SWP, and PAI), consistent with the conceptual framework presented in Fig. 2. This approach reduces dimensionality and focuses on physiologically meaningful drivers of yield and cracking. To capture temporal dynamics, predictors were defined to represent plant physiological and water status at specific time points, with each variable reflecting the condition of an individual tree during key phenological periods. These time-specific PWS indicators (e.g., TG, SC, SWP, and PAI) were used as integrative descriptors of PWS, rather than as representations of UAV acquisition timing.

Variable importance scores were computed to quantify the contribution of each PWS indicator and its temporal occurrence (i.e., specific flight dates) to model predictions. This approach reduces dimensionality and focuses on physiologically meaningful drivers of yield and cracking. To capture temporal dynamics, predictors were defined to represent plant physiological and water status at specific time points, with each variable reflecting the condition of an individual tree during key phenological periods. These time-specific PWS indicators (e.g., TG, SC, SWP, and PAI) were used as integrative descriptors of plant state, rather than as representations of UAV acquisition timing. The irrigation treatment variable was included as a continous variable of the daily irrigation (mm day^{-1}) in the calibration dataset. The independent test dataset (control plots) represents an unseen irrigation regime, allowing evaluation of model transferability beyond the conditions used for training. Yield measurements, fruit cracking observations, and predicted PWS indicators were integrated into a unified database and randomly split into training (70%) and validation (30%) datasets. The 2025 growing season was excluded from model calibration and validation and was used exclusively as an independent test set to evaluate model performance under previously unseen seasonal conditions.

2.10. Clustering analysis

Yield and fruit cracking data were compiled for all trees across the two growing seasons. To identify groups of trees with similar yield and fruit-cracking trajectories, clustering analysis was applied. The optimal number of clusters was determined using the Calinski-Harabasz (CH) index (Caliński and Harabasz, 1974), which maximizes the ratio of between-cluster to within-cluster variability. Candidate solutions ranging from 2 to 10 clusters were evaluated using the *vegan* package in R (Oksanen et al., 2020). Tree grouping was subsequently performed using the Fuzzy C-Means (FCM) algorithm (Zhou et al., 2014), which assigns each tree partial membership values across clusters, allowing for gradual transitions between physiological states (Ohana-Levi et al., 2021, 2022; Peeters et al., 2024). Statistical differences among clusters in yield and fruit cracking were assessed using one-way ANOVA followed by Tukey's HSD post hoc tests, based on the sampled measurement trees (24 trees). The statistical analysis was conducted on the subset of the selected trees for which detailed physiological and yield measurements were available. Given the sampling design and spacing between measurement trees, spatial autocorrelation effects are expected to be limited. These trees were selected to represent the variability across irrigation treatments and orchard conditions, providing a consistent basis for comparing cluster-level differences. Relationships between cluster membership and the seasonal dynamics of PWS indicators were further examined to identify threshold conditions associated with increased fruit-cracking-related yield loss across the two growing seasons. By grouping trees with comparable physiological behavior and production outcomes, the clustering framework delineates orchard-scale management zones characterized by similar water-stress sensitivity and cracking risk.

3. Results

3.1. Climate and irrigation effects on the measured PWS, yield, and cracking rate

Seasonal climate conditions differed between the three study years (Fig. 3). In 2024, the season was characterized by more intense and prolonged heat stress, as reflected in higher mean daily air temperatures during the summer months than in 2023. In 2025, the season was characterized by intense short heatwaves. In addition, the number of heatwave days was highest in 2024 (83), middle in 2023 (65), and lowest in 2025 (18), indicating more persistent periods of elevated thermal stress. Minimum temperatures followed the expected seasonal cycle, with cooler winter conditions and strong summer–winter contrasts in both years. However, overall thermal conditions during the growing season were consistently higher in 2024. To mitigate increased atmospheric demand, irrigation inputs were elevated during summer 2024, resulting in the highest total seasonal irrigation amount (918 mm) compared to 2023 (739 mm) (Fig. 3). Despite considerably fewer heat waves in 2025, the total irrigation amount applied by the grower was relatively high (908 mm).

3.2. Plant water status indicators

The physiological responses varied significantly across treatments and seasons (Fig. 4). TG increased steadily during 2023, reaching higher cumulative values than in 2024, when growth was slower and more limited throughout the season. This reduction in cumulative growth coincided with the higher frequency of heatwaves and elevated temperatures in 2024. Under deficit irrigation (50% Early), periods of negative TG were observed, indicating temporary stem shrinkage and reduced growth rather than actual negative irrigation inputs (Fig. 4A). SWP reflected these differences, with the lowest values observed under deficit irrigation, especially in the early-deficit (50% Early) treatment, indicating increased plant water stress. SC values remained low during the summer months and increased toward autumn. In 2023, SC increased more uniformly across treatments (~0.04–0.06 mol m^{-2} s^{-1}), whereas in 2024, values were generally higher (~0.07–0.09 mol m^{-2} s^{-1}). In both years, SC was lowest under deficit irrigation, with the early-deficit treatment showing the strongest reduction in 2024, consistent with the elevated heat stress during this period (Fig. 4C).

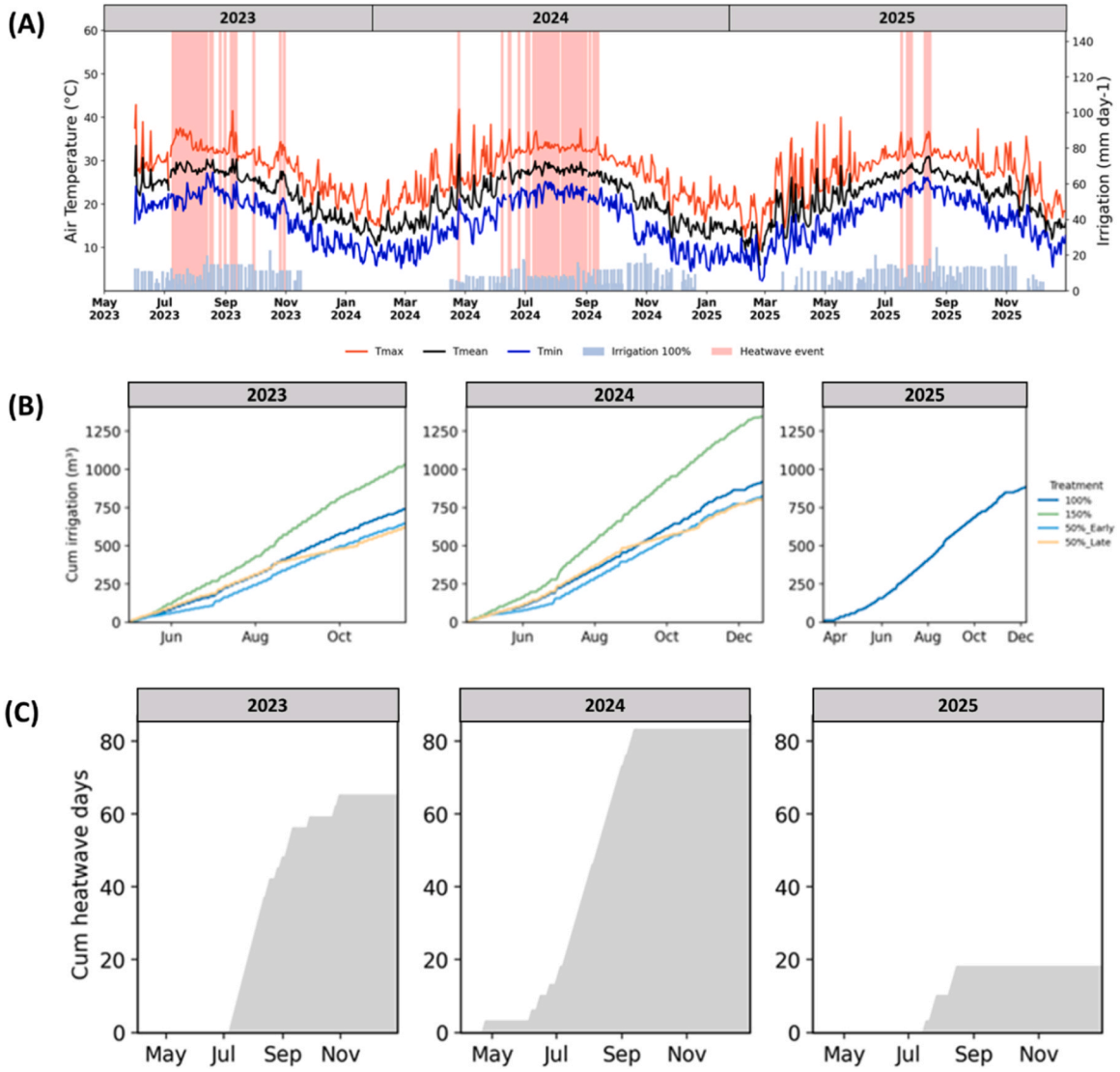

Fig. 3. Seasonal meteorological conditions and irrigation dynamics during the 2023, 2024, and 2025 growing seasons in relation to citrus phenological stages. (A) Temporal dynamics of soil moisture (light blue), maximum air temperature (red), mean air temperature (black), and minimum air temperature (blue). (B) Cumulative irrigation applied under each irrigation treatment. (C) Cumulative number of heatwave days recorded during the growing seasons.

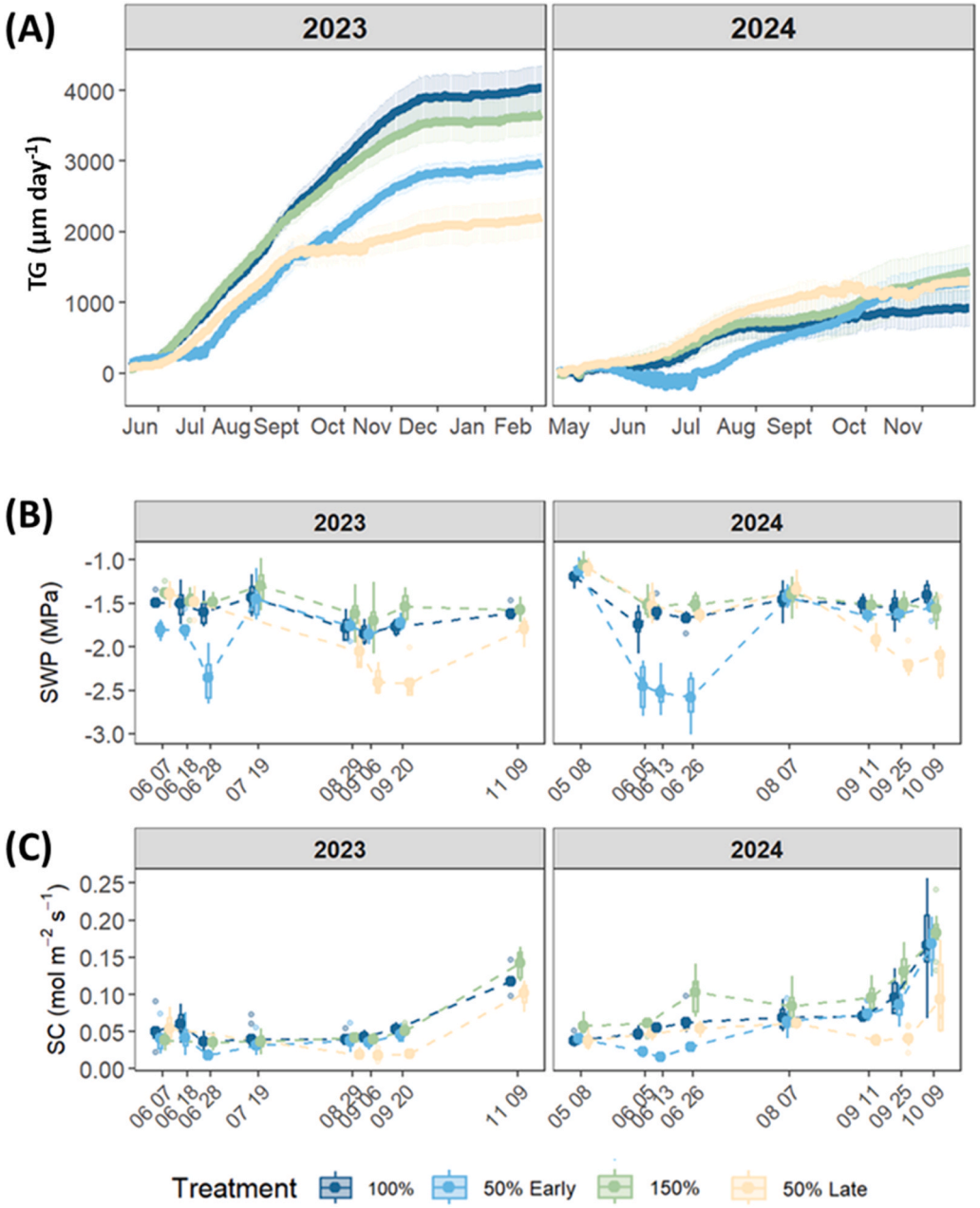

Fig. 4. Seasonal dynamics of plant water status (PWS) indicators during the 2023 and 2024 growing seasons. (A) Cumulative trunk growth rate (TG). (B) Stem water potential (SWP). (C) Stomatal conductance (SC). Colors represent irrigation treatments: dark blue- control (100%); green– over-irrigation (150%); light blue- early deficit irrigation (50% Early); and yellow - late deficit irrigation (50% Late).

3.3. Yield and fruit cracking

Fig. 5 summarizes the effects of irrigation treatments on fruit cracking rate (%) and yield (fruit trees^{-1}) across the 2023, 2024, and 2025 seasons. The three seasons differed markedly in productivity, with 2023 and 2025 representing off-crop years (~300 fruit trees^{-1} and ~125 fruit trees^{-1}, respectively, under standard irrigation), while 2024 was an on-crop year (~1300 fruit trees A^{-1}). In 2023, cracking rates were low (~3%) and did not differ significantly among treatments, indicating limited sensitivity to irrigation under low-fruit-load conditions. In contrast, in 2024, cracking rates increased substantially and showed clearer treatment effects. The standard irrigation treatment (100%) exhibited the highest cracking rate (~14%), whereas deficit irrigation treatments (50% Early and 50% Late) and excess irrigation (150%) showed lower cracking levels (~7–9%), with control being significantly different from 50% Late. Despite the higher cracking intensity, the highest yield in 2024 was observed under standard irrigation (100%), but it was not significantly higher than the 50% Late treatment. Deficient irrigation (50% Early) and excess irrigation (150%) resulted in reduced yield, which was significantly different than control and 50% Late treatments. The independent 2025 validation dataset exhibited an intermediate cracking incidence (~8% in the control treatment), providing an additional temporal test of model performance under climatic conditions that differed from both the low-cracking 2023 season (~3%) and the high-cracking 2024 season (~14%).

3.4. UAV-based prediction of PWS indicators using RF models

Across all three PWS indicators (TG, SWP, and SC), the RF model consistently outperformed XGBoost, ANN, and SVR, achieving the

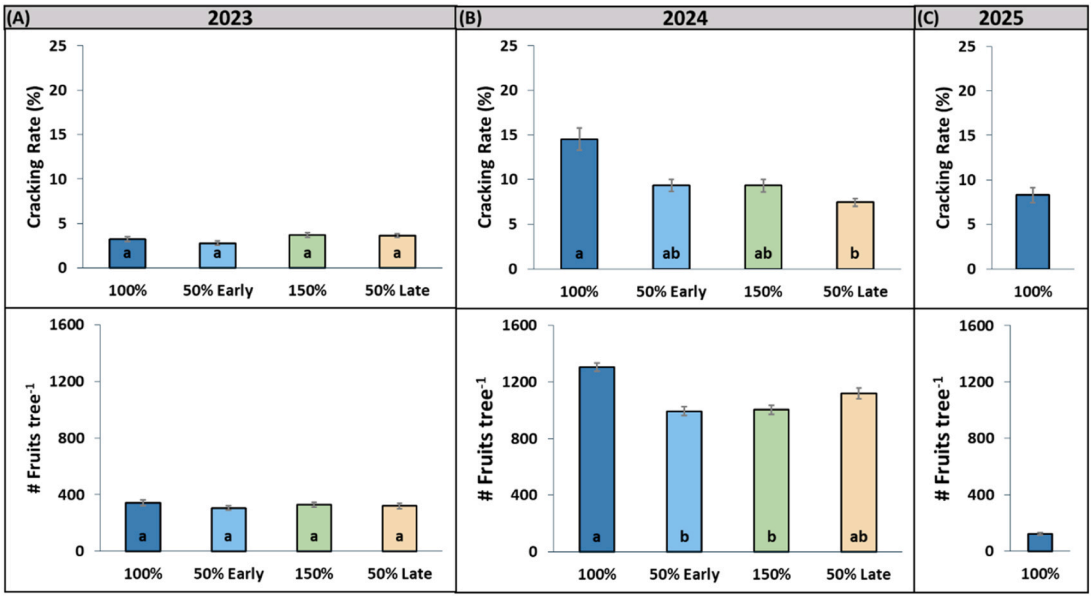

Fig. 5. Total fruit-cracking rate (top panels) and average yield per tree (bottom panels) under different irrigation treatments during the 2023–2025 growing seasons. Colors indicate irrigation treatments: dark blue = control (100% irrigation), green = over-irrigation (150%), light blue = early deficit irrigation (50% Early), and yellow = late deficit irrigation (50% Late).

highest validation performance and the lowest RMSE values (Table S3). While some models (e.g., ANN and XGBoost) showed comparable or higher calibration accuracy, RF demonstrated superior generalization, with more stable performance across validation and independent test sets. For TG, RF achieved a strong predictive performance (R^2_{cal}= 0.900 ± 0.028; R^2_{val} = 0.832 ± 0.063; $RMSE_{cal}$ = 0.709 ± 0.148 μm day^{-1}; $RMSE_{val}$ = 8.468 ± 1.691 μm day^{-1}), with consistent performance in the independent test dataset (R^2_{test} = 0.799; $RMSE_{test}$ = 7.349 μm day^{-1}). The most influential predictors included irrigation-related inputs and growing degree days (GDD), followed by relative humidity (RH), vegetation indices (NDVI, EVI), red-band reflectance (668 nm), canopy temperature (Tc), and temporal features (Fig. 6; Fig. S2).

For SWP, RF also showed high accuracy (R^2_{cal} = 0.926 ± 0.019; R^2_{val} = 0.856 ± 0.012; $RMSE_{cal}$ = 0.137 ± 0.066 MPa; $RMSE_{val}$ = 0.150 ± 0.048 MPa; R^2_{test} = 0.828; $RMSE_{test}$ = 0.112 MPa). Key predictors included mean NDVI, irrigation-related inputs, NIR reflectance (842 nm), canopy temperature (Tc), and reflectance in the green (560 nm) and red-edge (717 nm) bands, highlighting the combined influence of canopy condition and environmental drivers on plant water potential. For SC, predictive performance was similarly robust (R^2_{cal} = 0.945 ± 0.006; R^2_{val} = 0.851 ± 0.018; $RMSE_{cal}$ = 0.013 ± 0.005 mol m^{-2} s^{-1}; $RMSE_{val}$ = 0.030 ± 0.020 mol m^{-2} s^{-1}; R^2_{test} = 0.783; $RMSE_{test}$ = 0.014 mol m^{-2} s^{-1}). The most important predictors included GNDVI, GDD, red-edge reflectance (717 nm), elevation, and temporal features.

Overall, RF provided the most reliable and stable framework for estimating PWS indicators from UAV-derived features. The slightly lower predictive performance for SWP compared to TG likely reflects its higher short-term variability and sensitivity to recent environmental conditions, including irrigation timing. In contrast, SC predictions highlight the strong sensitivity of stomatal regulation to spectral information in the red-edge and NIR regions.

3.5. Prediction of yield and fruit cracking

For yield estimation, the RF model demonstrated strong predictive performance, with high agreement between observed and predicted values across calibration, validation and test datasets (Fig. 7; Fig. S3). Calibration performance was high (R^2_{cal} = 0.956; $RMSE_{cal}$ = 109.596 fruits tree^{-1}), and validation performance remained robust (R^2_{val}= 0.913; $RMSE_{val}$ = 174.613 fruits tree^{-1}), indicating good generalization across irrigation conditions and seasons. Bias values were low and negative in both calibration (−16.765 fruits tree^{-1}) and validation (−33.623 fruits tree^{-1}), suggesting a slight underestimation at higher yield levels without systematic bias. The test dataset demonstrated similarly robust performance, with R^2_{test} = 0.896, $RMSE_{test}$ = 183.134 fruits tree^{-1} , bias = −18.442 fruits tree^{-1} (Fig. S3A). Variable importance analysis (Fig. 7A) showed that mid-season physiological indicators were the dominant drivers of yield. Specifically, SC and SWP ranked as the most influential predictors in July, followed by TG. Structural canopy attributes, represented by PAI in July and September, contributed to yield prediction but with lower relative importance.

For fruit cracking estimation, the RF model also exhibited strong predictive performance (Fig. 7; Fig. S3), with calibration R^2_{cal} = 0.927 and $RMSE_{cal}$ = 1.460%, and validation R^2_{val} = 0.851 and $RMSE_{val}$ = 2.383%. Bias values were low in both calibration (−0.455%) and validation (−1.192%), indicating stable and largely unbiased predictions across the observed range of cracking intensities. The test dataset demonstrated similarly robust performance, with R^2_{test} = 0.845, $RMSE_{test}$ = 2.375%, and bias = 0.489% (Fig. S3B). Variable importance analysis identified SWP as the dominant predictor of fruit cracking, particularly during late-season conditions (September), followed by SWP in July. SC in both July and September showed moderate importance, while PAI contributed less to model performance (Fig. 7B).

Yield and fruit-cracking patterns exhibited clear spatial variability across the orchard (Fig. 8). In both seasons, areas of higher and lower yield formed distinct spatial gradients. In 2023, higher-yielding trees were distributed across specific zones of the orchard, while lower yields were observed in other areas. In 2024, overall yield levels increased, and zones of high productivity expanded, with large, contiguous areas exceeding 1200 fruits per tree. Fruit cracking showed a contrasting spatial distribution. In 2023, cracking rates were generally low (approximately 2–4%) but varied spatially across the orchard. In 2024, cracking increased substantially, with localized areas exceeding 15%, forming distinct spatial clusters of higher cracking intensity (Fig. 8).

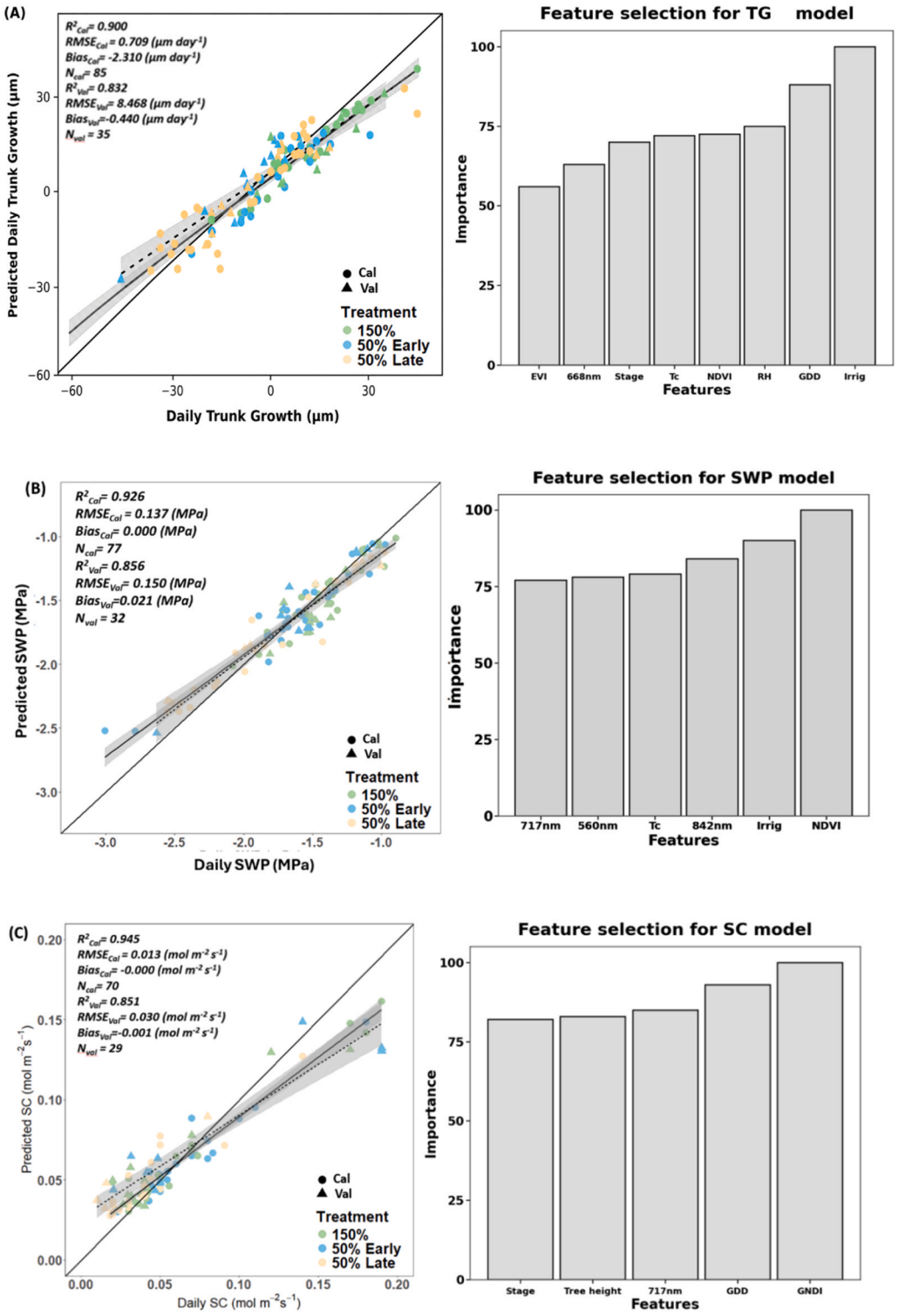

Fig. 6. Performance and variable importance of Random Forest (RF) models for estimating plant water status (PWS) indicators. Panels (A-C) show the relationship between measured and predicted values for trunk growth (TG), stem water potential (SWP), and stomatal conductance (SC), respectively, for the calibration, validation, and independent test datasets. Solid lines represent the 1:1 reference line, and dashed lines indicate linear regression fits for visualization purposes only. Model performance is quantified using the coefficient of determination (R^2) and root mean squared error (RMSE), calculated from model predictions. Panels (D-F) show the variable importance (VIP) scores from the RF models for TG, SWP, and SC, respectively. Predictor variables include UAV-derived spectral indices, canopy temperature (Tc), LiDAR-based structural metrics, and meteorological variables (e.g., GDD, RH), as defined in Table S1. Irrigation input is represented as a continuous variable (Irr, mm). Variable names and abbreviations are consistent with Table S1.

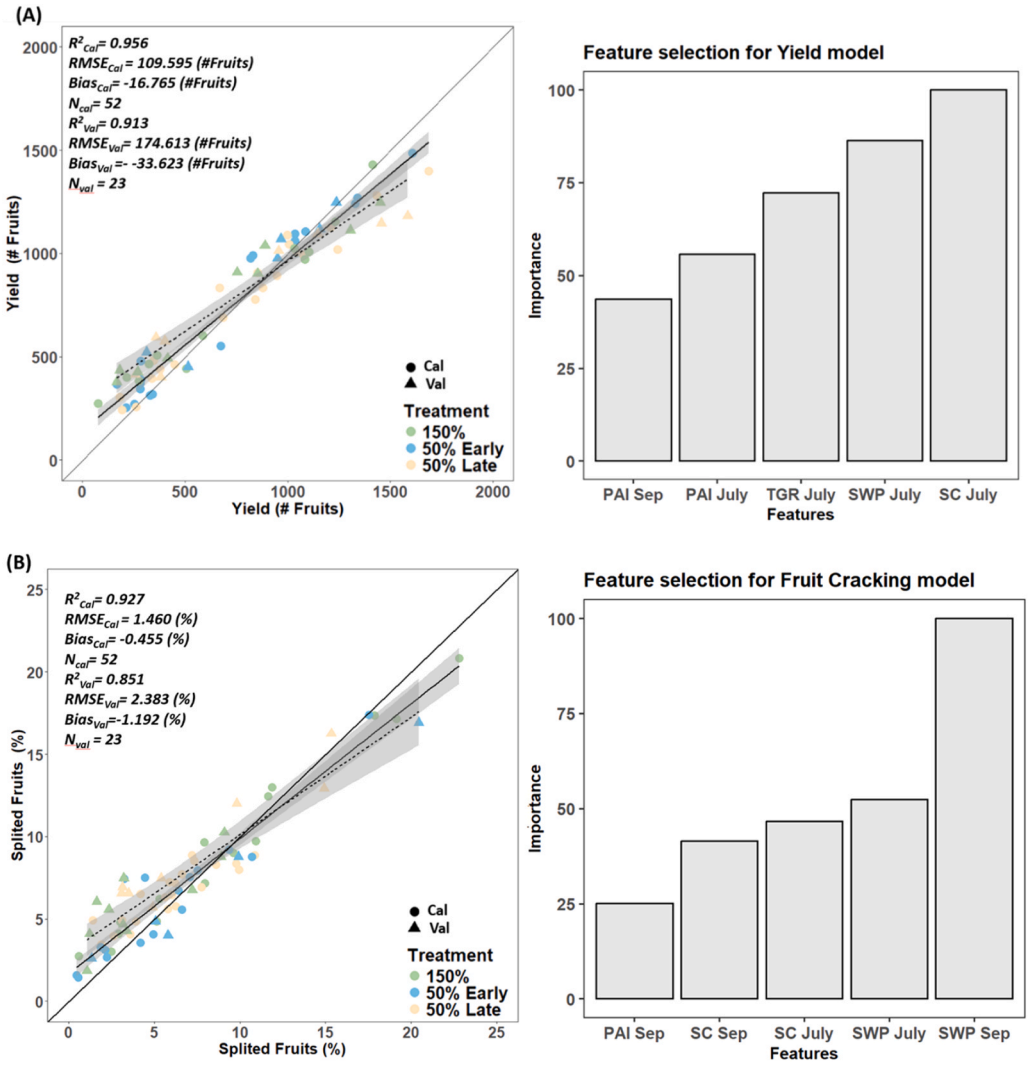

Fig. 7. UAV-based prediction of citrus yield and fruit cracking under different irrigation treatments (50% Early, 50% Late, 150%). (A) Yield (number of fruit trees^{-1}): observed versus predicted values for calibration (gray circles) and validation (gray triangles). The solid line represents the 1:1 line, and the dashed line shows the model fit. Feature importance analysis indicates that yield prediction was primarily driven by July stomatal conductance (SC), July stem water potential (SWP), July trunk growth rate (TG), and plant area index (PAI) in July and September. (B) Fruit cracking (%): relationships between observed and predicted values for calibration and validation datasets. Feature selection analysis highlights July and September SWP and SC, together with September PAI, as the strongest predictors.

3.6. Clustering of yield and cracking

Despite these spatial patterns, statistical comparisons at the treatment level showed that yield and cracking did not differ significantly among irrigation treatments in 2023. In 2024, both yield and cracking were significantly higher under the standard (100%) irrigation treatment, while the remaining treatments did not differ significantly from one another. Remote sensing-based predictions from both years further indicated that yield and cracking patterns were not consistently aligned with irrigation treatments. To further characterize orchard-scale variability, clustering analysis was applied to identify groups of trees with contrasting yield and fruit-cracking trajectories across both growing seasons (Fig. 9). The clustering was based on a subset of 24 selected measurement trees, which were used to define cluster membership, and the resulting classification was projected across the orchard. In 2023, four yield clusters and three cracking clusters were identified, whereas in 2024, three clusters were identified for both yield and cracking. The clusters showed clear spatial separation for both variables, except for yield in 2024, where the blue and yellow clusters were not clearly distinguishable.

Cluster-level statistics (mean ± standard error) are presented in Fig. 9. In 2024, yield was significantly higher in the yellow cluster than in the other clusters, and this cluster showed the lowest cracking values. In 2023, the yellow and blue clusters exhibited the highest yields and cracking values. Cracking clusters differed significantly in SWP (Fig. S4). In 2023, the blue and yellow clusters showed more negative SWP values across most sampling dates. In 2024, the yellow cluster showed higher cracking and lower SWP values than the other clusters. Temporal SWP patterns in 2024 showed that the yellow cluster maintained SWP values below approximately −1.6 MPa during most measurement dates (Fig. S4).

4. Discussion

This study advances UAV-based irrigation and water-stress research by moving beyond canopy stress detection toward a physiology-based interpretation of fruit cracking. While earlier studies primarily focused on estimating water status or predicting yield from spectral and thermal indicators, the present framework explicitly links temporal PWS dynamics during key phenological stages with cracking-associated yield loss at the tree scale. A central contribution of this work is the integration of multispectral, thermal, LiDAR, physiological, and environmental

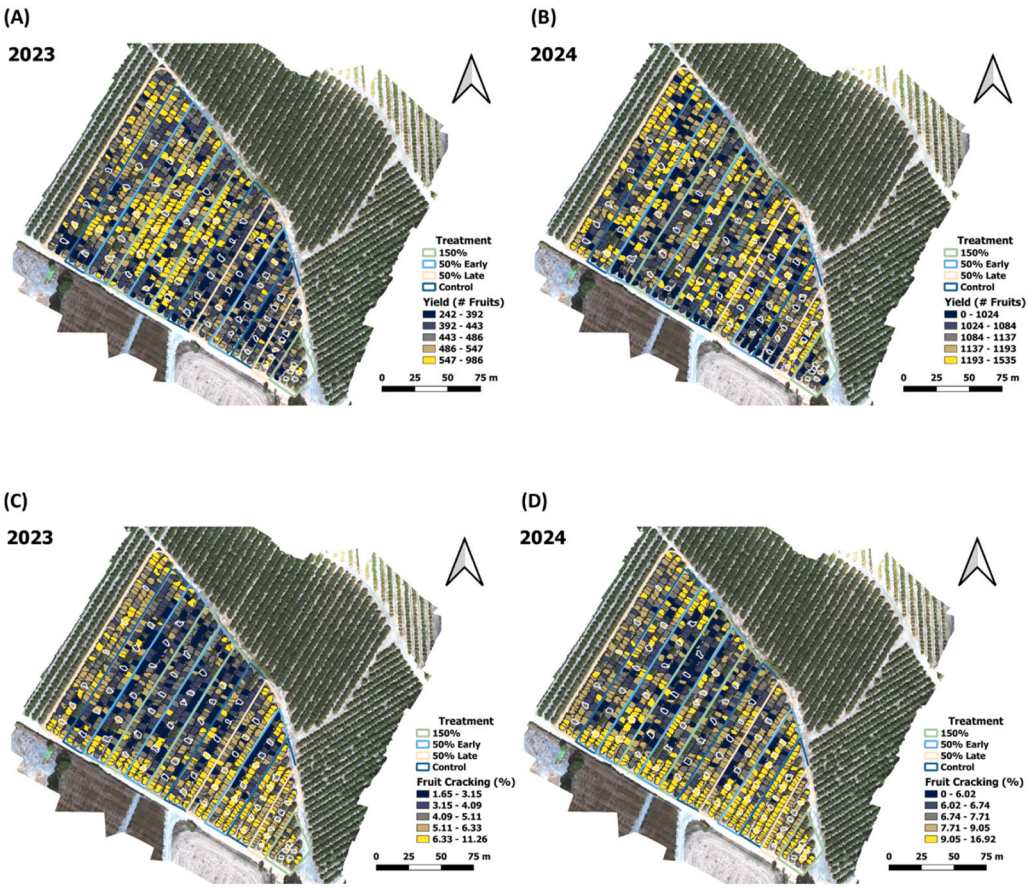

Fig. 8. Spatial distribution of citrus yield and fruit cracking under different irrigation regimes (50% Early, 50% Late, 150%, and Control) in 2023 and 2024. (A-B) Yield (number of fruit trees^{-1}) for 2023 and 2024. (C-D) Fruit cracking rate (%) for 2023 and 2024. Maps highlight strong treatment-driven heterogeneity: high irrigation (150%) consistently increased yield but was also associated with increased cracking, whereas deficit irrigation (50% Early and 50% Late) reduced yield but also contributed to localized reductions in cracking severity.

data within a modeling framework, in which UAV-derived variables were first translated into physiologically meaningful PWS indicators and then related to agronomic outcomes. This approach improves interpretability compared with direct sensor-to-yield models and supports a mechanistic understanding of how temporal hydraulic instability contributes to fruit cracking under varying irrigation and climatic conditions. The results further demonstrate that cracking variability was associated not only with irrigation amount but also with temporal fluctuations in SWP, SC, and TG under periods of elevated atmospheric demand. These findings highlight the importance of monitoring dynamic PWS trajectories rather than relying solely on static or end-of-season stress indicators.

Three main findings emerge. First, UAV-based RF models reliably predicted multiple PWS indicators across two contrasting seasons, highlighting the complementary roles of spectral, thermal, and structural information in capturing plant hydraulic responses. Second, mid-season PWS indicators (July–September) were the strongest predictors of both yield and fruit cracking, corresponding to the fruit enlargement phase (Stage III), when rapid pulp expansion coincides with a progressive reduction in peel thickness and structural resistance, increasing the likelihood of mechanical failure (Kaur et al., 2025; Yuying Wang et al., 2021). Third, clustering of yield and cracking trajectories revealed clear interannual differences: in the milder 2023 season, low yields were associated with minimal cracking, whereas in the hotter 2024 season, more negative SWP coincided with higher cracking levels despite increased irrigation inputs. Together, these findings indicate that citrus fruit cracking is governed by the interaction between atmospheric demand, plant hydraulic status, and canopy development, rather than by irrigation amount alone. To our knowledge, this is among the first studies to directly link UAV-based multi-sensor PWS predictions with fruit cracking outcomes at the tree scale, providing a scalable, physiology-based framework for precision irrigation management under increasing climatic variability.

4.1. *Linking PWS monitoring to climatic and irrigation drivers*

Climatic variability and irrigation inputs exerted strong controls on PWS indicators (TG, SWP, SC) across the two study seasons. In 2023, lower atmospheric demand, reflected in fewer heatwave days (65 vs. 83 in 2024) and lower mean temperatures, resulted in relatively moderate declines in PWS, with SWP generally remaining above −1.3 to −1.5 MPa for most of the season (Fig. S4). In contrast, in 2024, frequent heatwaves and sustained temperatures exceeding 35 °C increased atmospheric demand, leading to more pronounced reductions in SWP (often below −1.6 MPa), reduced TG, and altered SC dynamics despite higher irrigation inputs (Fig. 4; Fig. S4). These observations indicate that climatic conditions, particularly atmospheric demand, played a dominant role in shaping seasonal PWS dynamics beyond irrigation volume alone. Elevated SC and reduced SWP during peak heat periods suggest increased transpiration demand and hydraulic stress, which have been associated with enhanced fruit susceptibility to cracking under fluctuating water conditions (Barry and Bower, 1997; García-Luis et al., 1994; Li and Chen, 2017; Singh et al., 2020; Spada et al., 2024).

Irrigation timing further influenced these responses. Early-season deficit irrigation resulted in persistently lower SWP values and slower recovery during subsequent growth stages, whereas higher irrigation

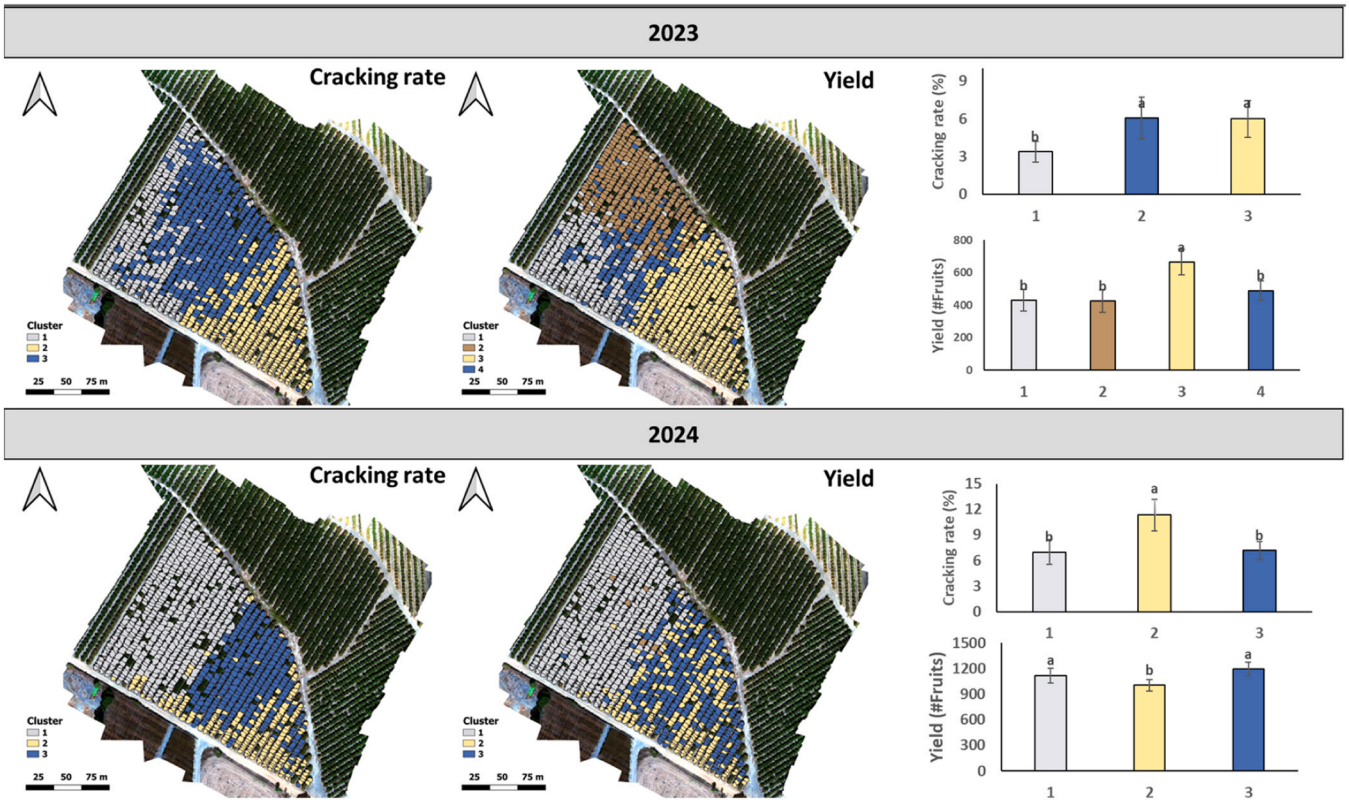

Fig. 9. Spatial clustering of fruit cracking rate and yield across the orchard in 2023 (top) and 2024 (bottom). The left panels show tree-level clusters of cracking rates, and the middle panels show corresponding yield clusters derived from fuzzy c-means clustering. Right panels summarize mean cracking rate (%) and yield (number of fruits per tree) for each cluster (mean ± SE). Different letters indicate significant differences among clusters within each year (ANOVA with Tukey's HSD, $p < 0.05$). Spatial patterns reveal consistent yield–cracking trade-offs across seasons, with high-yield clusters generally associated with higher cracking incidence, particularly under wetter conditions in 2024.

inputs promoted greater canopy development (Fig. 5). Although not directly reflected in treatment-level statistics, previous studies have shown that excessive or rapidly changing water availability can increase cracking incidence by amplifying fruit turgor pressure (Fischer et al., 2021; Zur et al., 2017). Together, these results demonstrate that the interaction between atmospheric demand and irrigation timing governs PWS dynamics. These findings underscore that effective irrigation management must account for temporal PWS dynamics under variable climatic demand, rather than relying solely on cumulative water inputs.

Total yield does not seem to affect cracking intensity. In 2023 and 2025, an off-crop year, cracking was very low (3%), in 2024, an on-crop year, cracking was 14% and in 2025, an extremely off-crop year, cracking intensity was around 8% (all in 100% irrigation, Fig. 5). The effect of irrigation on cracking intensity could be inferred by comparing the years and from 2024 data. In 2024 and 2025, irrigation was approximately 25% higher than in 2023, associated with induced cracking during these years. In 2024, cracking intensity was reduced in 50% Late treatment as compared to control, supporting the hypothesis that reduced irrigation reduces cracking intensity. However, cracking intensity in the 150% irrigation regime, applied throughout the season, was not induced, as might be expected, which deserves further investigation. The results demonstrate that fruit cracking was influenced not only by the amount of irrigation but also by the temporal stability of PWS during sensitive phenological stages. Although higher irrigation was applied in 2024 and 2025, the incidence of cracking increased under stronger heat stress and atmospheric demand, suggesting that maintaining stable physiological conditions may be more important than increasing total water input alone. These findings support a shift toward physiology-based precision irrigation strategies in which UAV-derived PWS monitoring is used to identify high-risk zones and optimize irrigation timing and intensity at the orchard scale.

4.2. *Value of UAV-based multi-sensor integration for PWS*

A central contribution of this study is demonstrating that UAV sensors fusion of thermal, multispectral, and LiDAR data can accurately estimate PWS indicators and relate them to yield and fruit cracking. Compared to single-sensor approaches, this multi-sensor framework provides a more comprehensive representation of canopy function by capturing complementary physiological, biochemical, and structural processes. Thermal imagery provided canopy temperature (Tc) and enabled the estimation of crop water stress, which is closely linked to stomatal regulation and PWS (Idso et al., 1981; Cohen et al., 2015; Katz et al., 2023). Multispectral data, particularly in the red-edge and near-infrared regions, captured variations in chlorophyll content and canopy condition (Dorigo et al., 2007; Haboudane et al., 2004; Ballester et al., 2019). LiDAR-derived structural metrics, including canopy area and PAI, supplied key information on canopy architecture and density that cannot be resolved by optical sensors alone (Ahmadi et al., 2019; Ustin and Middleton, 2021; Fang et al., 2019). The complementary contributions of these data sources were reflected in model performance: spectral red-edge features were most influential for SC prediction, thermal variables contributed strongly to SWP estimation, and structural metrics improved yield prediction via canopy attributes. Across sensors, time-series analysis consistently identified July-September as the period with the highest explanatory power, corresponding to the fruit enlargement phase. Overall, UAV-based multi--sensor integration provides a scalable approach for linking tree-level physiological measurements with orchard-scale variability. This approach enables continuous, spatially explicit monitoring of PWS,

providing a foundation for data-driven irrigation management under heterogeneous field conditions.

To incorporate temporal information, PWS indicators from multiple phenological stages and measurement dates were included as candidate predictors in the feature-selection and modeling framework. Thus, variables such as SWP, SC, TG, and PAI measured during different months were evaluated simultaneously, allowing the models to identify the most informative stage-specific physiological predictors of yield and fruit cracking. The selected July and September PWS indicators should therefore be interpreted as integrative physiological signals associated with critical fruit-development stages rather than as isolated single-date effects. However, the current framework does not explicitly model time-series dependence, lag effects, or cumulative stress trajectories, which remain important directions for future research using higher-frequency observations and dynamic modeling approaches.

4.3. Possible physiological understanding underlying cracking

The strong predictive performance of the RF models for PWS (R^2_{test} = 0.79, 0.82, and 0.78 for TG, SWP, and SC, respectively) highlights the tight coupling between plant water relations and fruit cracking. These indicators reflect complementary physiological processes that together govern fruit susceptibility to cracking. TG integrates cambial growth and internal water storage dynamics, representing the balance between carbon assimilation and water availability (Steppe et al., 2006; Dietrich et al., 2018; Sevanto, 2017). Periods of rapid TG during fruit enlargement indicate accelerated tissue expansion, which may increase internal fruit pressure. In this study, reduced TG in 2024 coincided with more negative SWP values and increased cracking levels (~14% vs. ~3% in 2023), suggesting a shift in growth-water balance under higher atmospheric demand. Seasonal changes in cracking intensity are not presented here, but it should also be considered that temporal fluctuations in water availability and TG may also affect the number of cracked fruits (Mesejo et al., 2016).

SWP, which integrates soil water availability and atmospheric demand, emerged as a key indicator associated with cracking patterns. Clustering analysis showed that trees with higher cracking consistently exhibited more negative SWP values (Li and Chen, 2017; Khadivi-Khub, 2014). Cracking-prone clusters in 2024 maintained SWP values below approximately −1.6 MPa for most of the measurement period, whereas less-affected trees remained above this range (Fig. S4). This indicates that both the magnitude and persistence of low SWP are associated with an increased incidence of cracking. SC provided additional insight into canopy-scale regulation of water loss (Horton and Hart, 1998; Kozlowski and Pallardy, 1997). Predicted SC values were higher in 2024 (~0.07–0.09 mol m^{-2} s^{-1}) compared to 2023 (~0.04–0.06 mol m^{-2} s^{-1}), reflecting increased transpiration demand under hotter conditions. Elevated SC may enhance water flux into the fruit, promoting pulp expansion and increasing mechanical stress on the peel when elasticity is limited (Holtzhausen, 1981). Finally, PAI linked the canopy structure to both productivity (Xu et al., 2023; Dian et al., 2023; Avioz et al., 2025), and cracking. Higher PAI values were associated with higher yield but also coincided with increased cracking in specific clusters, indicating that canopy size modulates the interaction between assimilate supply, hydraulic demand, and fruit-level stress. Together, these results indicate that fruit cracking emerges from the interaction between growth dynamics, PWS, and atmospheric demand, rather than from a single controlling factor.

4.4. Clustering and yield trade-offs

Clustering analysis identified distinct groups of trees characterized by different combinations of PWS, yield, and fruit cracking across seasons. In the milder 2023 season, clusters showed relatively low cracking levels (~3%) across the orchard, with limited differentiation among groups. Yield variability was also lower, consistent with the off-crop condition. In contrast, during the hotter 2024 season, clusters showed clearer separation, with higher yields (~1200–1400 fruits $tree^{-1}$) and increased cracking (~10–15%) observed in specific groups. These clusters were associated with more negative SWP values, frequently below −1.6 MPa, and higher transpiration conditions, as reflected by elevated SC. Despite increased irrigation inputs in 2024, these patterns persisted, indicating that spatial variability in PWS and climatic conditions contributed to the observed differences among clusters. The clustering results further showed that yield and cracking did not follow a uniform pattern across the orchard. In 2024, higher-yielding clusters were not consistently associated with lower cracking, whereas in 2023, both yield and cracking remained relatively low across clusters. From a management perspective, the spatial coherence of clusters suggests that canopy-level variability can be grouped into distinct zones with similar physiological and production characteristics. Such zone-based approaches may improve water-use efficiency by aligning irrigation inputs with spatial variability in PWS and production. Although the additional 2025 test set improved confidence in the models' temporal robustness, further validation across orchards, cultivars, and climatic regions is still required. In addition, heat stress was interpreted as a likely contributing seasonal factor associated with elevated fruit-cracking risk, although formal temperature and PWS interaction analysis was beyond the scope of the current study.

4.5. Implications for precision irrigation, limitations, and future work

By linking mid-season PWS dynamics to yield and fruit cracking outcomes, this study provides a scalable, tree-resolved framework for precision irrigation. UAV-based monitoring captures intra-orchard variability and enables the delineation of physiologically meaningful management zones, supporting irrigation decisions based on plant status and phenological sensitivity rather than uniform water application. This represents a step toward operational, climate-smart, zone-based irrigation management (Capel et al., 2017; Khadivi-Khub, 2014). Several limitations should be considered. First, UAV acquisitions were conducted at discrete time intervals (monthly), which may not fully capture short-term PWS fluctuations during extreme events such as heatwaves or irrigation pulses (Fang et al., 2019; Wang and Fang, 2020). Second, the study was conducted over three seasons at a single site and cultivar, limiting the generality of the findings across different climatic conditions and orchard systems. Third, LiDAR-derived PAI included both leaf and woody components, preventing separation between leaf area index (LAI) and woody area index (WAI), which may influence the interpretation of canopy and water relations. Finally, although the ML models showed strong predictive performance, they remain data-driven and do not explicitly represent underlying physiological processes.

Future work should address these limitations by incorporating higher-frequency monitoring, expanding the analysis across multiple years, cultivars, and climatic regions, and integrating UAV observations with satellite data for broader spatial coverage. In addition, coupling ML approaches with mechanistic or digital twin models may improve robustness and interpretability under extreme conditions. Such developments would support the transition toward adaptive irrigation strategies that dynamically respond to PWS and environmental variability. This integrated approach provides a foundation for next-generation irrigation management systems that combine real-time sensing with predictive modeling to optimize water use and crop performance.

Conclusions

A central finding of this study is that fruit cracking was more strongly associated with temporal PWS dynamics than with irrigation amount alone. Across seasons, higher cracking levels were observed under more negative SWP (often below ~−1.6 MPa), elevated atmospheric demand, and periods of rapid fruit growth. These findings support a shift from

volume-based irrigation management toward a physiology-driven approach that accounts for dynamic plant responses to environmental variability. In this context, UAV-derived PWS mapping enables spatially explicit monitoring of orchard heterogeneity and supports the delineation of management zones for site-specific irrigation. Importantly, the results indicate that reducing cracking risk depends on maintaining stable PWS trajectories during critical phenological stages, particularly mid- to late-season fruit development. This shifts irrigation management from a volume-based approach toward a physiology-driven strategy that accounts for plant responses to environmental variability. The integration of UAV-based multi-sensor data with physiological indicators enables spatially explicit monitoring of orchard heterogeneity and supports the delineation of management zones. This provides a practical pathway toward precision irrigation strategies that optimize water use, stabilize yield, and improve fruit quality. Overall, this framework offers a transferable approach for adaptive orchard management under increasing climatic variability and has potential applications across perennial cropping systems prone to water-stress-related disorders.

CRediT authorship contribution statement

Moshe (Vladislav) Dubinin: Writing – review & editing, Writing – original draft, Visualization, Validation, Software, Resources, Methodology, Investigation, Formal analysis, Data curation, Conceptualization. **Michael Morozov:** Data curation. **Ohaliav Keisar:** Data curation. **Guy Lidor:** Data curation. **Victor Alchanatis:** Writing – review & editing, Project administration, Funding acquisition. **Avi Sadka:** Writing – review & editing, Writing – original draft, Validation, Resources, Project administration, Methodology, Investigation, Funding acquisition, Data curation, Conceptualization. **Tarin Paz-Kagan:** Writing – review & editing, Writing – original draft, Visualization, Validation, Supervision, Resources, Project administration, Methodology, Investigation, Funding acquisition, Formal analysis, Data curation, Conceptualization.

Declaration of Generative AI and AI-assisted technologies in the writing process

During the preparation of this manuscript, the authors used ChatGPT to improve language and readability. All text generated with the assistance of this tool was carefully reviewed and revised by the authors, who take full responsibility for the final content of the publication.

Declaration of Competing Interest

The authors declare that they have no known competing financial interests or personal relationships that could have appeared to influence the work reported in this paper.

Acknowledgments

This study was funded by the European Union under the Horizon Europe programme (Grant Agreement No. 101086300, CrackSense). The views and opinions expressed are those of the authors only and do not necessarily reflect those of the European Union or the granting authority. Neither the European Union nor the granting authority can be held responsible for them. The authors gratefully acknowledge the orchard growers for granting access to their fields and facilitating data collection. We thank Yaniv Saville for his assistance with data collection and fieldwork.

Appendix A. Supporting information

Supplementary data associated with this article can be found in the online version at doi:10.1016/j.agwat.2026.110634.

Appendix B. Supporting information

Supplementary data associated with this article can be found in the online version at doi:10.1016/j.agwat.2026.110634.

Data Availability

Data will be made available on request.

References

Abekasis, D., Sadka, A., Rokach, L., Shiff, S., Morozov, M., Kamara, I., Paz-Kagan, T., 2024. Explainable machine learning for revealing causes of citrus fruit cracking on a regional scale. Precis. Agric. 25 (2), 589–613. https://doi.org/10.1007/s11119-023-10084-y.

Ahmad, U., Alvino, A., Marino, S., 2021. A Review of Crop Water Stress Assessment Using Remote Sensing. Remote. Sens. https://doi.org/10.3390/rs13204155.

Ahmadi, B., Ahmadalipour, A., Tootle, G., Moradkhani, H., 2019. Remote Sensing of Water Use Efficiency and Terrestrial Drought Recovery across the Contiguous United States. Remote. Sens. 11 (6), 731.

Arrish, S. Suliman M.. 2014. "Overlapped and Shadowed Tree Crown Segmentation Based on HSI Color Model and Watershed Algoritim." Universiti Teknologi Malaysia.

Avioz, D., Linker, R., Raveh, E., Baram, S., Paz-Kagan, T., 2025. Multi-Scale Remote Sensing for Sustainable Citrus Farming: Predicting Canopy Nitrogen Content Using UAV-Satellite Data Fusion. Smart Agric. Technol., 100906

Ballester, C., Brinkhoff, J., Quayle, W.C., Hornbuckle, J., 2019. Monitoring the Effects of Water Stress in Cotton Using the Green Red Vegetation Index and Red Edge Ratio. Remote. Sens. https://doi.org/10.3390/rs11070873.

Barry, G.H., Bower, J.P., 1997. Manipulation of Fruit Set and Stylar-End Fruit Split in 'Nova' Mandarin Hybrid. Sci. Hortic. 70 (2), 243–250. https://doi.org/10.1016/S0304-4238(97)00025-3.

Blanco, V., Blaya-Ros, P.J., Torres-Sánchez, R., Domingo, R., 2022. Irrigation and Crop Load Management Lessen Rain-Induced Cherry Cracking. Plants. https://doi.org/10.3390/plants11233249.

Bo, L., Guan, H., Mao, X., 2023. Diagnosing Crop Water Status Based on Canopy Temperature as a Function of Film Mulching and Deficit Irrigation. Field Crops Res. 304, 109154. https://doi.org/10.1016/j.fcr.2023.109154.

Boyaci, S., Kocięcka, J., Atilgan, A., Liberacki, D., Rolbiecki, R., Saltuk, B., Stachowski, P., 2024. Evaluation of Crop Water Stress Index (CWSI) for High Tunnel Greenhouse Tomatoes under Different Irrigation Levels. Atmosphere. https://doi.org/10.3390/atmos15020205.

Caliński, T., Harabasz, J., 1974. A Dendrite Method for Cluster Analysis. Commun. Stat. -Theory Methods 3 (1), 1–27.

Capel, C., Yuste-Lisbona, F.J., López-Casado, G., Angosto, T., Cuartero, J., Lozano, R., Capel, J., 2017. Multi-Environment QTL Mapping Reveals Genetic Architecture of Fruit Cracking in a Tomato RIL Solanum lycopersicum × S. Pimpinellifolium Population. Theor. Appl. Genet. 130 (1), 213–222. https://doi.org/10.1007/s00122-016-2809-9.

Chatterjee, S., Baath, G., Sapkota, B.R., Flynn, K.C., Smith, D.R., 2025. Enhancing LAI Estimation Using Multispectral Imagery and Machine Learning: A Comparison between Reflectance-Based and Vegetation Indices-Based Approaches. Comput. Electron. Agric. 230, 109790. https://doi.org/10.1016/j.compag.2024.109790.

Cho, S.B., Soleh, H.M., Choi, J.W., Hwang, W.-H., Lee, H., Cho, Y.-S., Cho, B.-K., Kim, M. S., Baek, I., Kim, G., 2024. Recent Methods for Evaluating Crop Water Stress Using AI Techniques: A Review. Sensors. https://doi.org/10.3390/s24196313.

Choi, J.-H., Lee, B.H.N., Gu, M., Lee, U.-Y., Kim, M.-S., Jung, S.-K., Choi, H.-S., 2020. Course of Fruit Cracking in 'Whansan' Pears. Hortic. Environ. Biotechnol. 61 (1), 51–59. https://doi.org/10.1007/s13580-019-00200-1.

Cohen, Y., Alchanatis, V., Sela, E., Saranga, Y., Cohen, S., Meron, M., Bosak, A., et al., 2015. Crop Water Status Estimation Using Thermography: Multi-Year Model Development Using Ground-Based Thermal Images. Precis. Agric. 16 (3), 311–329. https://doi.org/10.1007/s11119-014-9378-1.

Cronjé, P.J.R., Stander, O.P.J., Theron, K.I., 2013. Fruit Splitting in Citrus. Hortic. Rev. Vol. 41 177–200. https://doi.org/10.1002/9781118707418.ch04.

Dahro, B., Li, C., Liu, J.-H., 2023. Overlapping Responses to Multiple Abiotic Stresses in Citrus: From Mechanism Understanding to Genetic Improvement. Hortic. Adv. 1 (1), 4. https://doi.org/10.1007/s44281-023-00007-2.

Dian, Y., Liu, X., Hu, L., Zhang, J., Hu, C., Liu, Y., Zhang, J., et al., 2023. Characteristics of Photosynthesis and Vertical Canopy Architecture of Citrus Trees under Two Labor-Saving Cultivation Modes Using Unmanned Aerial Vehicle (UAV)-Based LiDAR Data in Citrus Orchards. Hortic. Res. 10 (3), uhad018. https://doi.org/10.1093/hr/uhad018.

Dietrich, L., Zweifel, R., Kahmen, A., 2018. Daily Stem Diameter Variations Can Predict the Canopy Water Status of Mature Temperate Trees. Tree Physiol. 38 (7), 941–952. https://doi.org/10.1093/treephys/tpy023.

Dorigo, W.A., Zurita-Milla, R., de Wit, A.J.W., Brazile, J., Singh, R., Schaepman, M.E., 2007. A Review on Reflective Remote Sensing and Data Assimilation Techniques for Enhanced Agroecosystem Modeling. Int. J. Appl. Earth Obs. Geoinf. 9 (2), 165–193. https://doi.org/10.1016/j.jag.2006.05.003.

Drucker, H., Chris, C., Kaufman, L., Smola, A., Vapnik, V., 2003. Support Vector Regression Machines. Adv. Neural Inf. Process. Syst. 9 (ember).

Efrat, N., Dubinin, V. (M.), Baram, S., Paz-Kagan, T., 2025. Modeling Seasonal Water Status and Predicting Yield in Almond Orchards Using UAV Multi-Sensor and

Meteorological Data. Agric. Water Manag. 320, 109868. https://doi.org/10.1016/j.agwat.2025.109868.
Fang, H., Baret, F., Plummer, S., Schaepman-Strub, G., 2019. An Overview of Global Leaf Area Index (LAI): Methods, Products, Validation, and Applications. Rev. Geophys. 57 (3), 739–799.
Fischer, G., Balaguera-López, H.E., Álvarez-Herrera, J., 2021. Causes of Fruit Cracking in the Era of Climate Change. A Review. Agron. Colomb. 39 (2), 196–207.
Friedman, J.H., 2001. Greedy Function Approximation: A Gradient Boosting Machine. Ann. Stat. 29 (5), 1189–1232. http://www.jstor.org/stable/2699986.
Galindo, A., Rodríguez, P., Collado-González, J., Cruz, Z.N., Torrecillas, E., Ondoño, S., Corell, M., Moriana, A., Torrecillas, A., 2014. Rainfall Intensifies Fruit Peel Cracking in Water Stressed Pomegranate Trees. Agric. For. Meteorol. 194, 29–35. https://doi.org/10.1016/j.agrformet.2014.03.015.
García-Luis, A., Duarte, A.M.M., Porras, I., García-Lidón, A., Guardiola, J.L., 1994. Fruit Splitting in 'Nova' Hybrid Mandarin in Relation to the Anatomy of the Fruit and Fruit Set Treatments. Sci. Hortic. 57 (3), 215–231. https://doi.org/10.1016/0304-4238(94)90142-2.
Gonzalez-Dugo, V., Zarco-Tejada, P.J., Fereres, E., 2014. Applicability and Limitations of Using the Crop Water Stress Index as an Indicator of Water Deficits in Citrus Orchards. Agric. For. Meteorol. 198199 94–104. https://doi.org/10.1016/j.agrformet.2014.08.003.
Gonzalez-Dugo, V., Zarco-Tejada, P., Nicolás, E., Nortes, P.A., Alarcón, J.J., Intrigliolo, D.S., Fereres, E., 2013. Using High Resolution UAV Thermal Imagery to Assess the Variability in the Water Status of Five Fruit Tree Species within a Commercial Orchard. Precis. Agric. 14 (6), 660–678. https://doi.org/10.1007/s11119-013-9322-9.
Groß, J., 2003. Variance Inflation Factors. R. N. 3 (1), 13–15.
Gupta, S.K., Bantawa, P., Rai, S., Ali, S., Pradhan, J., Lama, S.B., Rai, R., 2024. Enhancing Citrus Resilience: Strategies and Advances in Abiotic Stress Management: A Review. Indian. J. Agric. Res. 58.
Haboudane, D., Miller, J.R., Pattey, E., Zarco-Tejada, P.J., Strachan, I.B., 2004. "Hyperspectral Vegetation Indices and Novel Algorithms for Predicting Green LAI of Crop Canopies: Modeling and Validation in the Context of Precision Agriculture.". Remote. Sens. Environ. 90 (3), 337–352. https://doi.org/10.1016/j.rse.2003.12.013.
Hassanpour, R., Majnooni-Heris, A., Fakheri Fard, A., Tasumi, M., 2024. Spatio-Temporal Monitoring of Plant Water Status Using Optical Remote Sensing Data and in Situ Measurements. Adv. Space Res. 74 (10), 4688–4704. https://doi.org/10.1016/j.asr.2024.07.049.
Hoaglin, D.C., Iglewicz, B., 1987. Fine-Tuning Some Resistant Rules for Outlier Labeling. J. Am. Stat. Assoc. 82 (400), 1147–1149. https://doi.org/10.1080/01621459.1987.10478551.
Holtzhausen, L.C., 1982. Creasing: Formulating a Hypothesis. In: Proceedings of the International Society of Citriculture, 1981, 1. Fruit Tree Research Station.
Hornik, K., Stinchcombe, M., White, H., 1989. Multilayer Feedforward Networks Are Universal Approximators. Neural Netw. 2 (5), 359–366. https://doi.org/10.1016/0893-6080(89)90020-8.
Horton, J.L., Hart, S.C., 1998. Hydraulic Lift: A Potentially Important Ecosystem Process. Trends Ecol. & Evol. 13 (6), 232–235. https://doi.org/10.1016/S0169-5347(98)01328-7.
Idso, S.B., Jackson, R.D., Pinter, P.J., Reginato, R.J., Hatfield, J.L., 1981. Normalizing the Stress-Degree-Day Parameter for Environmental Variability. Agric. Meteorol. 24, 45–55. https://doi.org/10.1016/0002-1571(81)90032-7.
Katimbo, A., Rudnick, D.R., DeJonge, K.C., Lo, T.H., Qiao, X., Franz, T.E., Nakabuye, H. N., Duan, J., 2022. Crop Water Stress Index Computation Approaches and Their Sensitivity to Soil Water Dynamics. Agric. Water Manag. 266, 107575. https://doi.org/10.1016/j.agwat.2022.107575.
Katz, L., Ben-Gal, A., Litaor, M.I., Naor, A., Peeters, A., Goldshtein, E., Lidor, G., et al., 2023. How Sensitive Is Thermal Image-Based Orchard Water Status Estimation to Canopy Extraction Quality? Remote. Sens. https://doi.org/10.3390/rs15051448.
Kaur, K., Gupta, M., Rattanpal, H.S., Anand, S., Singh, G., Raina, D., 2025. Impact of Meteorological Parameters in Fruit Splitting of Daisy Mandarin under Subtropical Conditions. Front. Plant. Sci. 16. https://www.frontiersin.org/journals/plant-science/articles/10.3389/fpls.2025.1700833.
Khadivi-Khub, A., 2014. Physiological and Genetic Factors Influencing Fruit Cracking. Acta Physiol. Plant. 37 (1), 1718. https://doi.org/10.1007/s11738-014-1718-2.
Kizel, F., L. Bruzzone, and J.A. Benediktsson. 2017. "Simultaneous Empirical Line Calibration of Multiple Spectral Images." In *2017 IEEE International Geoscience and Remote Sensing Symposium (IGARSS)*, 4185–88. https://doi.org/10.1109/IGARSS.2017.8127924.
Kozlowski, T.T., Pallardy, S.G., 1997. CHAPTER 12 - Transpiration and Plant Water Balance. edited by Theodore T Kozlowski and Stephen G B T - Physiology of Woody Plants (Second Edition) Pallardy. San Diego: Academic Press, pp. 269–308. https://doi.org/10.1016/B978-012424162-6/50029-6.
Krajewski, A., Ebert, T., Schumann, A., Waldo, L., 2022. Pre-Harvest Fruit Splitting of Citrus. Agronomy. https://doi.org/10.3390/agronomy12071505.
Kuhn, M., 2015. A Short Introduction to the Caret Package. R. Found. Stat. Comput.
Kursa, M.B., Jankowski, A., Rudnicki, W.R., 2010. Boruta–a System for Feature Selection. Fundam. Inform. 101 (4), 271–285.
Kursa, M.B., Rudnicki, W.R., 2010. Feature Selection with the Boruta Package. J. Stat. Softw. 36 (11 SE-Articles), 1–13. https://doi.org/10.18637/jss.v036.i11.
Larcher, W., 2003. Physiological Plant Ecology: Ecophysiology and Stress Physiology of Functional Groups. Springer Science & Business Media.
Li, J., Chen, J., 2017. Citrus Fruit-Cracking: Causes and Occurrence. Hortic. Plant. J. 3 (6), 255–260. https://doi.org/10.1016/j.hpj.2017.08.002.
Li, S., Dai, L., Wang, H., Wang, Y., He, Z., Lin, S., 2017. Estimating Leaf Area Density of Individual Trees Using the Point Cloud Segmentation of Terrestrial LiDAR Data and a Voxel-Based Model. Remote. Sens. 9 (11), 1202.
Liu, Q., Wu, Z., Cui, N., Zheng, S., Zhu, S., Jiang, S., Wang, Z., Gong, D., Wang, Y., Zhao, L., 2024. Soil Moisture Content Estimation of Drip-Irrigated Citrus Orchard Based on UAV Images and Machine Learning Algorithm in Southwest China. Agric. Water Manag. 303, 109069. https://doi.org/10.1016/j.agwat.2024.109069.
Matsuki, K., Kuperman, V., Van Dyke, J.A., 2016. The Random Forests Statistical Technique: An Examination of Its Value for the Study of Reading. Sci. Stud. Read. 20 (1), 20–33. https://doi.org/10.1080/10888438.2015.1107073.
Mesejo, C., Reig, C., Martínez-Fuentes, A., Gambetta, G., Gravina, A., Agustí, M., 2016. Tree Water Status Influences Fruit Splitting in Citrus. Sci. Hortic. 209, 96–104. https://doi.org/10.1016/j.scienta.2016.06.009.
Morris, J., Mann, L., Collopy, J., 1998. Transpiration and Canopy Conductance in a Eucalypt Plantation Using Shallow Saline Groundwater. Tree Physiol. 18 (8–9), 547–555. https://doi.org/10.1093/treephys/18.8-9.547.
Nehemy, M.F., Benettin, P., Asadollahi, M., Pratt, D., Rinaldo, A., McDonnell, J.J., 2019. "How Plant Water Status Drives Tree Source Water Partitioning.". Hydrol. Earth Syst. Sci. Discuss. 2019 (October), 1–26. https://doi.org/10.5194/hess-2019-528.
Nemera, D.B., Dovjik, I., Florentin, A., Shahak, Y., Charuvi, D., Cohen, S., Sadka, A., 2023. Sparse-shading red net improves water relations in Valencia orange trees. Agric. Water Manag. 289, 108533.
Ogunbadewa, E.Y., 2012. Tracking Seasonal Changes in Vegetation Phenology with a SunScan Canopy Analyzer in Northwestern England. For. Sci. Technol. 8 (3), 161–172. https://doi.org/10.1080/21580103.2012.704971.
Ohana-Levi, N., Gao, F., Knipper, K., Kustas, W.P., Anderson, M.C., del Mar Alsina, M., Sanchez, L.A., Karnieli, A., 2021. Time-Series Clustering of Remote Sensing Retrievals for Defining Management Zones in a Vineyard. Irrig. Sci. 1–15.
Ohana-Levi, N., Zachs, I., Hagag, N., Shemesh, L., Netzer, Y., 2022. Grapevine Stem Water Potential Estimation Based on Sensor Fusion. Comput. Electron. Agric. 198 (July). https://doi.org/10.1016/j.compag.2022.107016.
Oksanen, J., Blanchet, F.G., Friendly, M., Kindt, R., Legendre, P., McGlinn, D., Minchin, P.R., O'Hara, R.B., Simpson, G.L., Solymos, P., 2022. Vegan: Community Ecology Package. R. Package Version 2, 5–7, 2020.
Park, S., Ryu, D., Fuentes, S., Chung, H., Hernández-Montes, E., O'Connell, M., 2017. Adaptive Estimation of Crop Water Stress in Nectarine and Peach Orchards Using High-Resolution Imagery from an Unmanned Aerial Vehicle (UAV). Remote. Sens. https://doi.org/10.3390/rs9080828.
Peeters, A., Cohen, Y., Bahat, I., Ohana-Levi, N., Goldshtein, E., Netzer, Y., Tenreiro, T.R., Alchanatis, V., Ben-Gal, A., 2024. A Spatial Machine-Learning Model for Predicting Crop Water Stress Index for Precision Irrigation of Vineyards. Comput. Electron. Agric. 227, 109578.
Puig-Sirera, À., Provenzano, G., González-Altozano, P., Intrigliolo, D.S., Rallo, G., 2021. Irrigation Water Saving Strategies in Citrus Orchards: Analysis of the Combined Effects of Timing and Severity of Soil Water Deficit. Agric. Water Manag. 248, 106773. https://doi.org/10.1016/j.agwat.2021.106773.
R Core, T., 2026. R: A Language and Enviroment for Statistical Comupting. R Foundation for Statistical Computing, Vienna, Austria.
Robinson, P.J., 2001. On the Definition of a Heat Wave. J. Appl. Meteorol. 40 (4), 762–775. https://doi.org/10.1175/1520-0450(2001)040<0762:OTDOAH>2.0.CO;2.
Romero, M., Luo, Y., Su, B., Fuentes, S., 2018. Vineyard Water Status Estimation Using Multispectral Imagery from an UAV Platform and Machine Learning Algorithms for Irrigation Scheduling Management. Comput. Electron. Agric. 147, 109–117. https://doi.org/10.1016/j.compag.2018.02.013.
Roussel, J.-R., Auty, D., Coops, N.C., Tompalski, P., Goodbody, T.R.H., Meador, A.S., Bourdon, J.-F., De Boissieu, F., Achim, A., 2020. LidR: An R Package for Analysis of Airborne Laser Scanning (ALS) Data. Remote. Sens. Environ. 251, 112061.
Sánchez-Virosta, A., Gómez-Candón, D., Montoya, F., Pérez-García, Y., Jiménez, V., Martínez-López, J.A., González-Piqueras, J., López-Urrea, R., Sánchez, J.M., 2025. Remote and Proximal Sensing Assessment of Water Status and Its Correlation with Yield on Almond Orchards in Southeast Spain. Precis. Agric. 26 (6), 92. https://doi.org/10.1007/s11119-025-10290-w.
Santos, M., Egea-Cortines, M., Gonçalves, B., Matos, M., 2023. Molecular Mechanisms Involved in Fruit Cracking: A Review. Front. Plant. Sci. 14 (March), 1–19. https://doi.org/10.3389/fpls.2023.1130857.
Seo, H.-J., Sawant, S.S., Song, J., 2022. Fruit Cracking in Pears: Its Cause and Management—A Review. Agronomy. https://doi.org/10.3390/agronomy12102437.
Sevanto, S.A., 2017. An Empirical Method That Separates Irreversible Stem Radial Growth from Bark Water Content Changes in Trees: Theory and Case Studies. Plant. Cell. & Environ. 40 (2), 290–303.
Sharma, P., Meyyazhagan, A., Easwaran, M., Sharma, M.M.M., Mehta, S., Pandey, V., Liu, W.-C., et al., 2022. Hydrogen Sulfide: A New Warrior in Assisting Seed Germination during Adverse Environmental Conditions. Plant. Growth Regul. 98 (3), 401–420. https://doi.org/10.1007/s10725-022-00887-w.
Shi, X., Wen, M., Dong, Z., Zhang, J., Srivastava, A.K., Moussa, M.G., Zhang, Y., 2025. Periodicity of Fruit Cracking in Orange Fruit and Integrated Management Intervention. Plants. https://doi.org/10.3390/plants14030389.
Singh, A., Shukla, A.K., Meghwal, P.R., 2020. Fruit Cracking in Pomegranate: Extent, Cause, and Management – A Review. Int. J. Fruit. Sci. 20 (sup3), S1234–S1253. https://doi.org/10.1080/15538362.2020.1784074.
Spada, P.L., Dominguez, E., Continella, A., Heredia, A., Gentile, A., 2024. Factors Influencing Fruit Cracking: An Environmental and Agronomic Perspective. Front. Plant. Sci. 15. https://www.frontiersin.org/journals/plant-science/articles/10.3389/fpls.2024.1343452.

Steppe, K., De Pauw, D.J.W., Lemeur, R., Vanrolleghem, P.A., 2006. A Mathematical Model Linking Tree Sap Flow Dynamics to Daily Stem Diameter Fluctuations and Radial Stem Growth. Tree Physiol. 26 (3), 257–273. https://doi.org/10.1093/treephys/26.3.257.

Tattersall, G.J. 2017. "Thermimage: Thermal Image Analysis." *CRAN. R-Project.*

Tukey, J.W., 1977. Exploratory Data Analysis, 2. Springer.

Ustin, S.L., Middleton, E.M., 2021. Current and Near-Term Advances in Earth Observation for Ecological Applications. Ecol. Process. 10 (1), 1. https://doi.org/10.1186/s13717-020-00255-4.

Velazquez-Chavez, L.J., Daccache, A., Mohamed, A.Z., Centritto, M., 2024. Plant-Based and Remote Sensing for Water Status Monitoring of Orchard Crops: Systematic Review and Meta-Analysis. Agric. Water Manag. 303, 109051. https://doi.org/10.1016/j.agwat.2024.109051.

Wang, Y., Fang, H., 2020. Estimation of LAI with the LiDAR Technology: A Review (MDPI AG). Remote. Sens.. https://doi.org/10.3390/rs12203457.

Wang, Y., Guo, L., Zhao, X., Zhao, Y., Hao, Z., Luo, H., Yuan, Z., 2021. Advances in Mechanisms and Omics Pertaining to Fruit Cracking in Horticultural Plants. Agronomy. https://doi.org/10.3390/agronomy11061045.

Wang, Y., Peng, J., Song, X., Leng, P., Ludwig, R., Loew, A., 2018. Surface Soil Moisture Retrieval Using Optical/Thermal Infrared Remote Sensing Data. IEEE Trans. Geosci. Remote. Sens. 56 (9), 5433–5442. https://doi.org/10.1109/TGRS.2018.2817370.

Xu, W., Yang, F., Ma, G., Wu, J., Wu, J., Lan, Y., 2023. Multiscale Inversion of Leaf Area Index in Citrus Tree by Merging UAV LiDAR with Multispectral Remote Sensing Data. Agronomy. https://doi.org/10.3390/agronomy13112747.

Zhang, K., Chen, S.-C., Whitman, D., Shyu, M.-L., Yan, J., Zhang, C., 2003. A Progressive Morphological Filter for Removing Nonground Measurements from Airborne LIDAR Data. IEEE Trans. Geosci. Remote. Sens. 41 (4), 872–882.

Zhou, K.L., Fu, C., Yang, S.L., 2014. Fuzziness parameter selection in fuzzy c-means: The perspective of cluster validation. Sci. China Inf. Sci. 57 (11), 1–8. https://doi.org/10.1007/s11432-014-5146-0.

Ziegler, Y., Grote, R., Alongi, F., Knüver, T., Ruehr, N.K., 2024. Capturing Drought Stress Signals: The Potential of Dendrometers for Monitoring Tree Water Status (November). Tree Physiol., tpae140. https://doi.org/10.1093/treephys/tpae140.

Zur, N., Shlizerman, L., Ben-Ari, G., Sadka, A., 2017. Use of Magnetic Resonance Imaging (MRI) to Study and Predict Fruit Splitting in Citrus. Hortic. J. 86 (2), 151–158. https://doi.org/10.2503/hortj.MI-147.